

---

# Hearing the Unspoken: Language Model Priors for Acoustic Adversarial Attacks

---

**Jiani Xie**  
University of Melbourne  
jiani.xie1@unimelb.edu.au

**Andrew C. Cullen**  
University of Melbourne

**Paul Montague**  
DST Group

**Benjamin I. P. Rubinstein**  
University of Melbourne

## Abstract

Automatic Speech Recognition (ASR) systems operating in real-time settings must process acoustic input under strict temporal constraints, where transcription decisions are inherently made on incomplete information. This causal constraint serves as an information bottleneck on attackers, significantly limiting attack performance. Our new Semantic Gambit attack breaks this causal limitation by augmenting the adversary with predictive context derived from a Large Language Model in real-time. Our experiments show that this form of augmentation can elevate the corpus-level Word Error Rate to 35.6%—a three-fold increase over the current state-of-the-art. Ultimately, this work reveals how common, low-latency LLM tooling can be exploited to systematically subvert real-time ASR pipelines.

## 1 Introduction

Modern Automatic Speech Recognition (ASR) systems are vulnerable to adversarial perturbations, which, when overlaid on speech, degrade the resulting transcription (1; 2; 3). Crucially, attack performance is proportional to the information available to the attacker—the more the attacker knows about the target utterance, the more precisely the perturbation can be shaped to disrupt it. In offline settings, this is no obstacle, since the attacker can condition on the full utterance; however, real-time settings require the attack to coincide with speech, sharply limiting available information. In this real-time setting, the attacker faces a hard information constraint, in that the attacker can only access information from *before* the attack is deployed (4). The moment the perturbation is injected, it distorts the acoustic environment, foreclosing further clean observation and bounding accessible information.

We circumvent this information bound with the **Semantic Gambit** (SG), which exploits a secondary information channel to improve attack performance. The bound applies only to the acoustic modality: while future speech cannot be heard, the partial transcript of what has already been spoken is often sufficient for a Large Language Model (LLM) to predict what comes next. A multimodal generator then fuses this predicted continuation with the acoustic prefix to produce an input-specific perturbation in real time (Figure 1). To the best of our knowledge, this is the first attack framework to use LLM-based predictions to guide perturbation generation in a different modality.

We evaluate Semantic Gambit against Wav2Vec 2.0 (5) across a range of realistic operating conditions. At its strongest configuration, the system elevates the victim model’s word error rate from 2% to over 35% under a realistic 20 dB SNR constraint, approximately three times the degradation achieved by the best baseline. Ablations confirm that semantic conditioning contributes up to 20 percentage points beyond what acoustic context alone provides, and the full pipeline generates a 3-second perturbation in just 0.6 seconds on average, operating at roughly 5× real-time without specialist optimization—fast enough to attack live speech with latency to spare. That such results are possible demonstrates that our

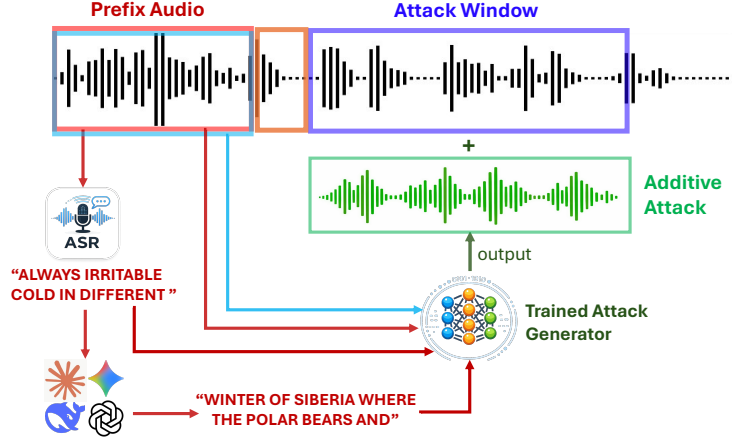


Figure 1: **Overview of Attack Pathways.** In streaming attacks, a prefix audio segment is exploited by a generator to construct an attack in the attack window. Our SG attack enhances information availability by supplementing audio information with prefix audio, an ASR transcript of the prefix, and an LLM forecast (red arrows), producing an information advantage over the current SOTA for such attacks (blue arrow). The orange box denotes the computational delay for synthesizing attacks.

understanding of the risks facing ASR models may have been significantly understated. More broadly, they suggest that defensive AI research must consider the potential for augmented information, lest we underestimate the risks facing models deployed in adversarially-exposed conditions.

## 2 Background Review: An Acoustic Taxonomy

Adversarial attacks on ASR systems can be classified by the information available to the attacker. In our review of this space, we have observed that an unacknowledged but key taxonomical distinction between attacks relates to the attacker’s knowledge. As such, we begin by formalizing the taxonomy of extant attacks through a unifying framework in which every attack is characterized by an *information filtration operator* that determines what portion of the target utterance is visible to the generator. As we will demonstrate in our experiments, there is an associated general hierarchy where increasing both the available information and the relevance of the information yields stronger attacks.

**General Formulation.** Let  $\mathcal{X} \subseteq \mathbb{R}^T$  denote the space of valid acoustic waveforms and let  $\mathcal{Y}$  be the space of token sequences. An ASR model is defined as the mapping  $M : \mathcal{X} \rightarrow \mathcal{Y}$ , which assigns a transcription  $y = M(x)$  to an input  $x \in \mathcal{X}$ . An adversarial attack seeks a perturbation  $\delta \in \mathcal{X}$  to maximize the divergence between the original transcription and the perturbed result  $y' = M(x + \delta)$ , typically measured via Word Error Rate (WER). To formalize the bounds on the attacker’s knowledge, we rely on the concept of a filtration—which represents the total information accumulated by the process up to a specific moment. Let  $\mathcal{F}_t = \sigma(x_1, \dots, x_t)$  denote the filtration of the clean signal and  $\mathcal{F}_t^W = \sigma(w_1, \dots, w_t)$  the observed filtration of the perturbed signal  $w = x + \delta$  at time  $t$ .

We characterize the attacker’s capability through an information operator  $H : \mathcal{X} \rightarrow \mathcal{Z}$ , where  $\mathcal{Z}$  denotes the observation space. A learned attack mechanism  $f_\theta : \mathcal{Z} \rightarrow \mathcal{X}$  produces the perturbation  $\delta = f_\theta(H(x))$ . The adversarial objective is thus:

$$\max_{f_\theta \in F(H)} \text{WER}(M(x), M(x + f_\theta(H(x)))) \quad (1)$$

where  $F(H)$  represents the class of appropriate structural constraints.

**Perfect Information.** The most permissive regime grants the attacker full access to the utterance,  $H(x) = x$ . This characterizes Projected Gradient Descent (PGD) style-attacks (1) and offline methods that optimize over the entire signal (6; 3). Here, the generator can iteratively refine  $\delta$  against the victim model. However, these attacks are *retroactive* by construction: by the time optimization terminates, the utterance has already been spoken.

**Hidden Information.** At the opposite extreme, universal attacks discard input dependence entirely,  $H(x) = \emptyset$ . A single perturbation is precomputed offline and applied to every utterance (7; 8). While sidestepping temporal constraints, this forces the perturbation to optimize for average-case degradation across the training distribution, foreclosing access to input-dependent victim vulnerabilities.

**Partial Information.** Real-world threats exist in the space between these extremes, where the attacker’s knowledge is limited by causal and environmental factors. In streaming settings, for example, the presence of the perturbation  $\delta$  induces a form of deleterious self-interference. As it is assumed that the attacker’s perturbation induces a non-invertible physical channel transformation, the underlying clean signal is obscured in an unrecoverable manner. This forces the information histories to diverge such that  $\mathcal{F}_t^W \subset \mathcal{F}_t$ , such that  $\delta \neq 0$  must induce a degradation in conditional entropies  $\mathcal{H}(x_t|\mathcal{F}_t^W) > \mathcal{H}(x_t|\mathcal{F}_t)$ . To practically model this, we define a *causal barrier*  $t_p$  where  $\delta_{t \leq t_p} = 0$ .

**Proposition 1** (Information Admissibility). *An attack is admissible with respect to a causal barrier  $t_p$  if the operator  $H(x)$  is  $\mathcal{F}_{t_p}$ -measurable. Crucially, while  $t_p$  bounds what the attacker can **measure**, it does not bound the set of **computable functions** of those measurements. For any  $\mathcal{F}_{t_p}$ -measurable function  $\phi$ , the operator  $H(x) = [x_p, \phi(x_p)]$  is admissible.*

To formalize this, we assume that the attacker observes the prefix  $H(x; t_p) = x \cdot \mathbb{1}[t < t_p]$ . Following the Neural Voice Camouflage attack of Chiquier et al. (4), we also assume that the attack requires a computation delay  $\tau$ , and targets a window of duration  $\Delta$ . The resulting perturbation is thus

$$\delta_t = f_{\theta,t}(H(x; t_p)), \quad t \in \{t_p + \tau, \dots, t_p + \tau + \Delta\} . \quad (2)$$

This framework captures the fundamental tension of real-time ASR attacks: the necessity of acting upon partial history while managing the informational loss induced by the attack itself.

**Attack Constraints.** In addition to the informational restriction imposed by  $H$ , the perturbation is typically constrained to be imperceptible to a human listener. In the vision literature, this is conventionally expressed as a magnitude bound on  $\delta$  under an  $\ell_p$  norm,  $\|\delta\|_p \leq \epsilon$ . In the audio domain, however,  $\ell_p$  bounds correlate poorly with human audibility (6; 9): the human ear is sensitive to energy rather than per-sample magnitude, so a perturbation that is small under  $\ell_p$  may still be clearly audible while one that is large under  $\ell_p$  may be masked entirely by the signal. Following work that grounds audio distortion in perceptual quantities (10; 8), we adopt the signal-to-noise ratio,

$$\text{SNR}(\delta, x) = 10 \log_{10}(\|x\|_2^2 / \|\delta\|_2^2) \geq \text{SNR}_{\text{tgt}} , \quad (3)$$

as a more faithful proxy for audibility.

### 3 Semantic Gambit: An Augmented Information Attack

Our information-driven taxonomy induces the question: if attack performance is correlated with information, how can an attacker improve the volume of information available to them? Traditionally, breaking the information barriers implicit to  $H$  in real-world circumstances would be impossible; however, the rise of LLMs presents an exciting opportunity. These models excel at constructing a viable snapshot of the future without breaking the causal barrier.

This is possible even though the acoustic channel is bound by the self-interference that increases entropy  $\mathcal{H}(x_t|\mathcal{F}_t^W)$ , the symbolic content of the prefix remains stable. As such, we extend the partial-information operator to expose both the acoustic prefix and a predicted linguistic continuation:

$$H(x) = [x_p, \tilde{T}(x)], \quad \tilde{T}(x) = M(x_p) \oplus L(M(x_p)) , \quad (4)$$

where  $x_p$  is the observed prefix,  $L$  is an LLM for future-text prediction, and  $\oplus$  denotes concatenation.

**Proposition 2** (Symbolic Invariance). *Let  $\delta$  be a perturbation emitted at time  $t > t_p$ . The textual channel  $\tilde{T}(x)$  is invariant to  $\delta$ , whereas the acoustic filtration  $\mathcal{F}_t^W$  is a function of  $\delta$ .*

The value of this invariance is central to our method. The acoustic channel is bound by the temporal requirement that the attacker cannot hear what has not been spoken, and cannot reliably discern information after the perturbation has been emitted. The textual channel  $\tilde{T}(x)$ , however, is purely  $\mathcal{F}_{t_p}$ -measurable; it requires no further audio and is immune to the acoustic degradation induced by

the emitted perturbation. Prior streaming attacks (11; 4) have implicitly restricted  $\phi$  to the identity, equating “available information” with “observed audio.” Semantic Gambit operates beyond these bounds by using pre-trained linguistic priors that an acoustic-only generator cannot access. **It breaks the information barrier not by hearing more, but by knowing more.**

### 3.1 Implementation

We now describe the concrete realization of the augmented operator  $H$  introduced in Section 3. Each utterance  $x$  is partitioned into four contiguous segments: the *prefix* signal  $x_p$  of length  $t_p$ , during which the attacker passively observes; the *delay* of length  $\tau$ , modeling the computational latency of the real-time pipeline; the *injection-window* signal  $x_*$  of fixed length  $\Delta_* = 3$  s, into which the perturbation is injected; and the *suffix* which corresponds to the remaining audio. The perturbation  $\delta$  is then defined over the same temporal window as  $x_*$ . The augmented filtration operator  $H(x) = [x_p, \tilde{y}_*]$ , where  $\tilde{y}_*$  is the ASR-transcribed prefix concatenated with an LLM-predicted continuation, depends on  $x$  only through the prefix  $x_p$ .

---

#### Algorithm 1 Semantic Gambit (SG) Training Procedure.

---

**Require:** Victim ASR  $M$ , language model  $L$ , generator  $G_\theta$ , training set  $\mathcal{D}$ , target SNR  $\text{SNR}_{\text{tgt}}$   
**Ensure:** Optimized generator parameters  $\hat{\theta}$

- 1: **for** epoch = 1, . . . ,  $E$  **do**
- 2:   **for** each utterance  $(x, y^{\text{gt}}) \in \mathcal{D}$  **do**
- 3:     Partition  $x$  into  $x_p$  and  $x_*$  per the fixed temporal schedule
- 4:      $y_p \leftarrow M(x_p)$ ;  $y_f \leftarrow L(y_p)$  ▷ Semantic expansion
- 5:      $\tilde{\delta} \leftarrow G_\theta(\text{MFCC}(x_p), E_{\text{sem}}(y_p \oplus y_f))$  ▷ Perturbation generation
- 6:      $\delta \leftarrow \text{SCALETOSNR}(\tilde{\delta}, x_*, \text{SNR}_{\text{tgt}})^\dagger$  ▷ Constraint enforcement
- 7:      $\theta \leftarrow \theta - \eta \nabla_\theta (-\mathcal{L}_{\text{CTC}}(M(x + \delta), y^{\text{gt}}))$  ▷ Optimization
- 8:   **end for**
- 9: **end for**
- 10: **return**  $\hat{\theta}$

---

<sup>†</sup>The SCALETOSNR operator applies a uniform scalar rescaling to match a prescribed perturbation budget; it does not feed target-window information into the generator. See Appendix A, § *Perturbation scaling*.

---

**Attack Pipeline.** The generator is a composition of three maps acting on the prefix. The victim ASR  $M$  produces a partial transcript  $y_p$ ; the language model  $L$  extends it into a forecast  $y_f$  of upcoming linguistic content, so that  $y_p \oplus y_f$  provides the text channel; and the multimodal generator  $G_\theta$  fuses acoustic features extracted by  $\text{MFCC}(\cdot)$  from the prefix audio with semantic embeddings produced by  $E_{\text{sem}}(\cdot)$  from the concatenated token sequence, yielding the raw perturbation  $\tilde{\delta}$  supported on the target interval, i.e., the time window into which the perturbation is injected. A rescaling under the target SNR constraint relative to  $x_*$  then produces the final  $\delta$ . End-to-end training maximizes the Connectionist Temporal Classification (CTC) loss (12) against the ground-truth transcript  $y^{\text{gt}}$ .

**Generator Architecture.**  $G_\theta$  has two stages. Stage 1 applies multi-modal self-attention jointly over audio frames and text tokens, letting the network learn which aspects of the linguistic forecast most inform the perturbation. Stage 2 is a Perceiver (13) that compresses this fused representation into a fixed-dimensional latent set, from which the perturbation waveform is decoded. Joint attention over both channels lets the perturbation be shaped by past ( $y_p$ ) and predicted ( $y_f$ ) speech simultaneously. Ablations comparing this design with three alternative fusion strategies are deferred to Appendix E.

**Code.** The full code required to replicate our experiment results can be found at <https://github.com/jnxie/semantic-gambit>.

## 4 Experiments

We evaluate Semantic Gambit along two axes. First, *attack efficacy across information regimes*: we benchmark SG against representatives of each regime from Section 2—a hidden-information universal perturbation and a white-noise control at the floor, an offline PGD attack with perfect-information

access at the ceiling, and partial-information methods that share the streaming constraint but differ in the information operator  $H$ . This design tests whether linguistic forecasting closes the gap to perfect-information performance without violating causality, decomposes any gain into acoustic, architectural, and semantic components, and verifies real-time feasibility via end-to-end latency. Second, *dataset transferability*: whether a generator trained on one corpus retains efficacy on held-out distributions. This isolates generalizable adversarial structure from corpus-specific overfitting and bounds the attack’s practical reach beyond the training distribution.

#### 4.1 Experimental Setup

Our primary experiments train and evaluate on the LibriSpeech corpus (14, CC BY 4.0 License): train-clean-100 (approximately 28,500 utterances) for training, dev-clean for validation and model selection, and test-clean for evaluation. Cross-dataset experiments additionally use Common Voice 25.0 English (15, CC0 1.0 License), training a separate generator under matched compute (Section 4.4). The default victim is a pre-trained Wav2Vec 2.0 base model (5, Apache 2.0 License) fine-tuned with CTC, achieving approximately 2% clean WER on test-clean; cross-model experiments substitute HuBERT-Large (16, Apache 2.0 License) and Whisper-small (17, MIT License) at evaluation time without retraining the generator (Section 4.5). The generator  $G_\theta$  contains approximately 7.3M parameters. Semantic forecasts are provided by Llama 3 8B (18, Meta Llama 3 Community License) quantized to 8-bit precision, serving as the language model  $L$  that produces up to 15 continuation tokens per prefix transcript  $y_p$ , which are decoded and re-tokenized at the character level before entering  $G_\theta$  (see Appendix A). All attacks are evaluated under a 20 dB SNR constraint.

We systematically vary two temporal parameters: the prefix length  $t_p \in \{1.0, 2.0, 3.0, 4.0\}$  s, which controls the volume of acoustic and linguistic context available to the attacker before it acts, and the injection delay  $\tau \in \{0.0, 0.5, 1.0\}$  s, which controls the recency of that information relative to the point at which the perturbation is injected. Concretely,  $t_p$  governs how much context the attacker can extract from the prefix, while  $\tau$  represents the processing time required to access the acoustic signal and pass it through the pipeline before the perturbation is ready. The range of tested delays allows us to understand the influence of information recency on attack performance; Appendix D reports hardware measurements confirming that the actual pipeline latency falls within this range. Together, this grid tests whether the value of linguistic forecasting persists as operational conditions tighten.

#### 4.2 Baselines

We compare Semantic Gambit against five reference points spanning the information regimes of Section 2. **White Noise**, matched in duration and SNR to our perturbations, verifies that degradation stems from adversarial optimization rather than simple acoustic masking. **AO\*** (4) is the original purely acoustic convolutional generator of Chiquier et al., the closest prior work in the streaming input-specific setting. **AO** retains SG’s full generator architecture and training procedure but zeroes the text channel, suppressing both the prefix transcription and the LLM continuation; any gap to SG is therefore attributable to linguistic anticipation rather than architectural differences. Following (19), **Universal** applies a single input-agnostic perturbation to every utterance, establishing a lower bound in the absence of input-specific information. **GT** replaces the LLM-generated forecast with the victim ASR’s own transcript of the target window, bounding efficacy under perfect semantic prediction. **PGD** (20) optimizes the perturbation with non-causal *access to the complete utterance*, providing a ceiling for purely gradient-based attacks that violate the streaming constraint. Implementation details and hyperparameters are deferred to Appendix B.

#### 4.3 Main Results

**Overall Efficacy.** Semantic Gambit achieves a roughly 17-fold increase in corpus-level WER over clean (2.05%  $\rightarrow$  35.63%) at its strongest operating point under a 20 dB SNR constraint, with sentence-level mean WER reaching 49.6% (Table 3). At every zero-delay configuration, SG exceeds even the offline PGD baseline despite PGD having non-causal access to the complete waveform and ground-truth transcript during optimization. SG operates under a strictly causal constraint—only the prefix audio is available at generation time—yet surpasses PGD, demonstrating that the linguistic channel compensates for the information deficit imposed by the streaming setting. This performance difference is indicative of the utility of providing the attacker with LLM-generated context, as this

additional information is enough to surpass the performance of an attack (PGD) that is able to look past the causal barrier. Furthermore, the white-noise control confirms that these gains reflect learned adversarial structure rather than acoustic masking.

Table 1: Corpus-level WER (%) under a 20 dB SNR constraint, with a 3.0 s target window. White noise produced negligible degradation (within 0.2% of clean) and is omitted. Bold marks the strongest attack per row among streaming-comparable methods (SG, AO, AO\*, Universal). Note that GT and PGD break the causality barrier, and as such is not directly comparable to the prefix attacks.

Prefix (s)	Delay (s)	Clean	SG	AO	AO*	Universal	GT (Bound)	PGD
1.0	0.0	2.05	<b>35.63</b>	15.15	12.23	17.37	23.53	17.01
	0.5	2.05	<b>16.26</b>	<b>19.57</b>	8.28	14.91	16.00	15.64
	1.0	2.02	<b>18.89</b>	14.52	5.34	17.21	21.42	14.58
2.0	0.0	2.02	<b>32.72</b>	12.58	2.16	14.45	19.01	14.46
	0.5	2.01	<b>20.32</b>	14.17	4.38	10.46	14.51	13.75
	1.0	2.03	<b>18.95</b>	13.42	3.19	10.62	23.40	13.17
3.0	0.0	2.03	<b>22.69</b>	14.82	4.27	13.14	16.47	13.21
	0.5	2.02	<b>21.17</b>	19.46	2.35	18.52	20.00	12.70
	1.0	2.01	<b>11.32</b>	11.11	8.45	9.99	12.94	12.02
4.0	0.0	2.01	<b>20.57</b>	19.85	5.80	10.05	12.44	12.18
	0.5	1.98	<b>19.12</b>	15.03	4.84	11.89	14.27	12.13
	1.0	1.97	<b>18.68</b>	17.68	8.78	11.15	14.46	11.56

**Information Hierarchy and Attack Effectiveness.** The three configurations, Universal, Acoustic-Only (AO), and Semantic Gambit, occupy progressively richer positions along the information axis constraining real-time ASR attacks, and their performance traces this hierarchy directly. At zero delay, averaging across prefix lengths, transitioning from the utterance-agnostic Universal attack (13.8% WER) to AO (15.6%) induces a modest gain, while transitioning from AO to SG (27.9%) yields a 79% relative increase, confirming that linguistic augmentation is the decisive factor. Universal’s ceiling is structural: a fixed perturbation forecloses access to input-dependent vulnerabilities, and the per-utterance signals it sees during training are averaged across the distribution, diluted past the point where any single input meaningfully shapes the perturbation. AO recovers per-utterance adaptivity, but acoustics are only one layer of what audio carries: AO observes the waveform alone, blind to the lexical and semantic structure that lives in the same signal. SG’s linguistic priors widen the information channel along two axes: the LLM extrapolates likely future content, and the prefix transcription itself supplies the generator with explicit linguistic context for crafting the perturbation. The augmentation pays off most at the strongest operating point (1.0 s prefix, zero delay), where SG yields a 135% relative increase over AO (35.63% vs. 15.15%), confirming that what governs real-time attack effectiveness is not what the attacker hears, but what it already knows.

**Effect of Prefix Length.** Across methods, attack efficacy decreases as the observed prefix grows longer: SG drops from 35.63% WER at a 1.0s prefix to 20.57% at 4.0s under zero delay, and the same trend appears in GT, PGD, and AO\*. Since PGD uses no text conditioning and AO\* uses no generator network, the effect cannot be attributed to the text pipeline alone. Two mechanisms appear to compound. First, longer prefixes give the victim a cleaner context to anchor its decoding, making later frames harder to perturb regardless of attack origin; this accounts for the baseline slope visible in PGD and AO\*. Second, for text-conditioned attacks, the forecast’s value depends on target predictability, which degrades with position as accumulated branching uncertainty outpaces the benefit of additional prefix conditioning. AO faces the victim-side mechanism but bypasses the text channel entirely, and its flat profile across prefix lengths isolates the text-specific decline as the dominant factor. Quantitatively, SG’s advantage over AO collapses from 20.5% at 1.0s to under 1% at 4.0s. We further rule out architectural and training considerations in Appendix F.

**Sensitivity to Injection Delay.** At every prefix length, zero injection delay produces the strongest attack, and performance broadly degrades monotonically as delay increases, as increasing delay forces the perturbation to target audio further removed from the last observed context without providing any compensating information. The purpose of the delay sweep is not to seek a better operating point but

to characterize the framework’s robustness under realistic computational latency, since any deployed streaming attack will incur non-zero processing time. The monotonic decline also confirms that the semantic conditioning is genuinely anchored to the temporal relationship between prefix and target rather than providing a generic, time-invariant boost. The sensitivity is more pronounced at shorter prefixes, where absolute performance is highest, and there is correspondingly more to lose.

**Relationship to the Ground-Truth Upper Bound.** At most operating points, and at every zero-delay configuration, Semantic Gambit surprisingly surpasses even the Ground-Truth (GT) oracle, which receives the full transcript rather than the conjunction of the transcription prefix and the associated LLM prediction. We believe that while SG operates at an information disadvantage, the LLM is likely introducing controlled divergence from the true transcript, avoiding overfitting by encouraging the generator to learn to disrupt a range of plausible decoding trajectories.

#### 4.4 Cross-Dataset Transferability

We train generators on LibriSpeech-100 (LS) (14) and Common Voice 25.0 English (CV) (15) independently under matched compute budgets and evaluate all four train–eval combinations. CV differs substantially from LS in speaker diversity, accent coverage, recording quality, and utterance length (Appendix G.1). Because the victim was pretrained on LS, clean WER on CV is 26% vs. 2% on LS; we report  $\Delta\text{WER}$  (attack WER – clean WER) to control for this baseline gap. The full numerical transferability matrix is in Appendix G.3.

**Attack Effectiveness Transfers Across Datasets.** The generator does not overfit to its training distribution. Figure 2 plots  $\text{ASR}@_\tau$  across the full threshold range for all four train–eval combinations. Comparing same-dataset (top row) and cross-dataset (bottom row) panels within each column, the curve shapes are nearly identical at every prefix: the generator produces the same distribution of per-utterance degradation severities regardless of whether it was trained on matched or mismatched data. On LS evaluation at prefixes 2.0–3.0 s, same-dataset and cross-dataset curves overlap across the full threshold range, with ASR values agreeing within 1 percentage point at both moderate ( $\tau=0.50$ ) and severe ( $\tau=1.00$ ) thresholds. On CV evaluation the match is tighter still, with curves virtually indistinguishable at prefixes 1.0–3.0 s. At prefix 4.0 s the relationship inverts: the cross-dataset generator trained on LS outperforms the matched CV-trained one, demonstrating that a mismatched but acoustically richer training set can surpass a matched but data-constrained one.

**Two Attack Regimes.** The exceedance curves also reveal that the two evaluation datasets occupy qualitatively different attack regimes. On LS, curves are concave with a steep initial drop and a long tail, reflecting a spread of degradation severities from mild to severe. On CV, curves plateau above 85% until  $\tau \approx 0.5$  before dropping, indicating near-universal disruption up to moderate severity. These correspond to partial-disruption and total-disruption regimes, respectively, driven by the victim’s baseline accuracy on each dataset. Crucially, transfer operates in both: the generator trained on mismatched data reproduces both the concave LS profile and the convex CV plateau.

**Prefix-Length Dependence Generalizes.** Within each panel of Figure 2, shorter prefixes consistently dominate longer ones at every threshold, and this ordering is preserved across datasets. This rules out accidental single-prefix transfer and indicates that the generator exploits properties of the victim architecture rather than dataset-specific acoustic patterns: prefix-length difficulty is determined by how the victim processes streaming audio, not by what the generator was trained on.

#### 4.5 Cross-Model Transferability

We next ask whether perturbations crafted against one victim ASR model retain effectiveness on an unseen model. We evaluate in a strict black-box transfer setting: the generator is trained against a single CTC surrogate and never updated; at test time, only the transcription model is substituted. We test bidirectional transfer within the CTC self-supervised family (between W2V2 and HuBERT-Large (16)) and cross-architecture transfer to Whisper-small (17), an encoder–decoder seq2seq model. Table 2 reports attack WER at delay 0.0 s alongside each surrogate’s in-domain baseline; the full prefix-by-delay grid is in Appendix H.

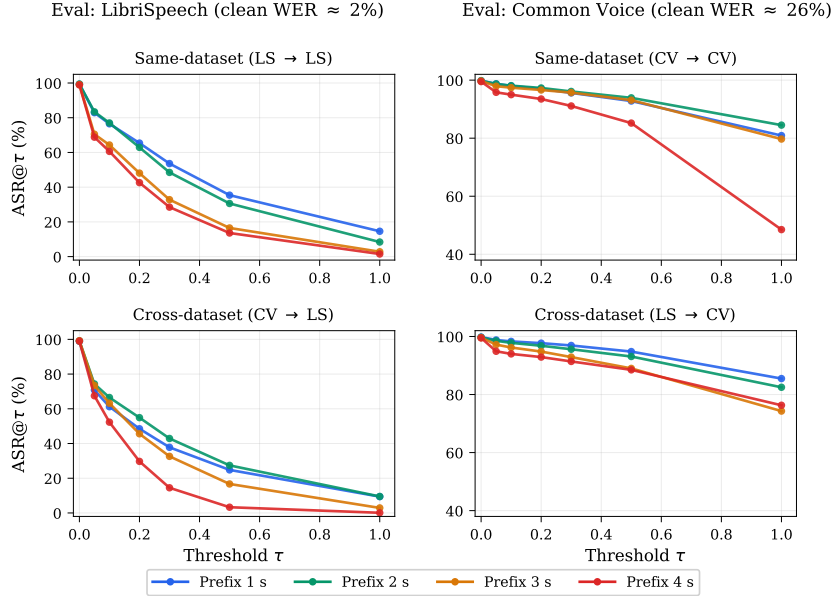


Figure 2: ASR@ $\tau$  exceedance curves for all four cross-dataset conditions at delay 0.0 s. Each panel shows four prefix configurations (colors). Top row: same-dataset training; bottom row: cross-dataset training. Left column: evaluation on LibriSpeech; right column: evaluation on Common Voice (**y-axis 40–100%, note different scale**). The correspondence between same-dataset and cross-dataset curves confirms that transfer preserves the full severity profile, not just attack rates at individual thresholds.

Table 2: Cross-model transfer attack WER (%) at delay 0.0 s and 20 dB SNR. “In-domain” is the surrogate evaluated on itself; “Transfer” is the same generator evaluated on the other CTC victim. Clean WER  $\approx 2\%$  on both models. Full results in Appendix H.

Prefix	W2V2 surrogate		HuBERT surrogate	
	In-domain	Transfer	In-domain	Transfer
1.0 s	35.63	19.05	21.21	11.97
2.0 s	32.72	19.04	25.17	3.85
3.0 s	22.69	11.57	14.64	7.41
4.0 s	20.57	9.14	14.97	6.74

**Perturbations Transfer Within the CTC Family.** Adversarial perturbations crafted against one CTC surrogate degrade an unseen CTC victim across every prefix configuration evaluated, with transfer attack WER reaching up to 19% against a 2% clean baseline (Appendix H.3). W2V2 and HuBERT share a raw-waveform CNN frontend, frame-level CTC decoding, and self-supervised pretraining objectives that encourage temporally localized representations, so perturbations exploiting fine-grained frame-level structure in one model find analogous structure in the other. Transfer is asymmetric, however: the W2V2 surrogate produces roughly twice the attack WER of HuBERT across configurations, plausibly because W2V2’s contrastive loss encourages linearly separable frame-level features whose adversarial directions generalize more readily, whereas HuBERT’s cluster-prediction objective produces more idiosyncratic decision boundaries. Thus, a single CTC surrogate, particularly W2V2, suffices to threaten the broader self-supervised CTC family.

**Transfer Does Not Cross the CTC–seq2seq Boundary.** Against Whisper-small, four independently designed attack methods all converge on attack WER within 1 percentage point of the 4% clean baseline, isolating the architectural boundary as the dominant factor (Appendix H.4). Whisper differs from the CTC models on every axis: its autoregressive decoder can override locally corrupted acoustic evidence using surrounding context; its supervised training on 680k hours of labeled audio encourages representations more robust to local distortions than frame-level self-supervised objectives; and its log-mel spectrogram front end occupies a fundamentally different input space from the raw-waveform

CNN shared by W2V2 and HuBERT. These results indicate that CTC and seq2seq systems present distinct robustness profiles requiring distinct threat models: perturbations that transfer freely within the CTC family are ineffective across the architectural boundary.

#### 4.6 Limitations and Future Work

Our focus within this work was to demonstrate the utility of LLM-guided augmentation in ASR attacks. We believe that this work lays the foundations for future explorations, including how resilient these attacks are in over-the-air attacks and in the presence of adaptive defenders. We also note that additional performance may be unlocked through updates to the LLM framework employed beyond our Llama 3 8B, especially given our 8-bit quantization with fixed token prediction lengths.

### 5 Related Work

**Audio-Specific Challenges** Audio adversarial attacks differ from image attacks in ways that complicate both design and evaluation. Standard  $\ell_p$  distances correlate poorly with perceived audibility, motivating perceptually grounded budgets such as SNR and psychoacoustic masking constraints (6; 9; 10). ASR systems also operate on diverse input representations, from raw waveforms to Mel spectrograms (21; 22), and a perturbation that appears small in one can become salient in another (23). Deployed pipelines additionally introduce microphone, room, and codec effects with no analogue in static image settings (24), and streaming deployments impose causal constraints.

**Attacks on ASR Systems** Early attacks on ASR pursued offline, targeted perturbations against end-to-end models (1; 24; 25), followed by universal variants that generalize across utterances (7; 19) and later incorporated EoT-based robustness and psychoacoustic objectives (26; 8). Most of these methods target older CTC or RNN-based architectures, and their findings do not obviously transfer to the stronger Transformer-based models that now dominate the field. Recent studies on Wav2Vec 2.0 and Whisper typically adopt standard gradient-based objectives within larger pipelines rather than proposing new attack methodologies (2; 27), and some sidestep transcription attacks entirely by manipulating task-level behavior, such as forcing Whisper to translate rather than transcribe (28). Few of these methods employ generative networks that map inputs to utterance-specific perturbations in a single forward pass; the only such work operating under causal streaming constraints, Neural Voice Camouflage (4) conditions solely upon acoustic information.

**Modern ASR Architectures** The ASR landscape has shifted rapidly in ways relevant to adversarial robustness. DeepSpeech 2 (29) paired recurrent encoders with a CTC (12) objective; Wav2Vec 2.0 (5) introduced self-supervised Transformer-based pre-training and became the de facto acoustic backbone; Whisper (17) scaled to encoder-decoder generation trained on roughly 680k hours of weakly supervised multilingual audio. Each generation brings different inductive biases and decoding mechanisms, so vulnerabilities established on one do not necessarily transfer to another. The present work targets Wav2Vec 2.0, whose sub-2% clean WER on LibriSpeech makes it a substantially harder target than the RNN-CTC systems evaluated by most prior adversarial work.

**Language Models as Auxiliary Components in Adversarial Systems** In prior works, LLM-generated paraphrases and synonym substitutions have been deployed against NLP classifiers (30), and stronger LLMs have served as autonomous red-team actors, that iteratively refine jailbreak prompts against other models (31). LLMs have also been adopted as evaluators during training and assessment (32), though this practice carries known issues with inconsistency, positional bias, and prompt sensitivity (33). In each of these roles, however, the language model either operates within the same modality as the attack or serves as an evaluation proxy. To our knowledge, no prior work has used a language model’s predictive capabilities to guide cross-modal attacks.

### 6 Conclusion

We reframe the information available to adversarial attackers by routing LLM-generated forecasts of upcoming linguistic content into a streaming perturbation generator. Changing the available information produces results that, operating in a true streaming regime, consistently surpass both acoustic-only streaming baselines and an offline gradient attacker with full waveform access.

Our results demonstrate that attack effectiveness scales with the informational content of the conditioning signal, with the largest gains where the audio bottleneck is tightest; perfect semantic prediction is not the optimal training signal, since the ground-truth oracle is itself surpassed by SG; and the prefix-length effect persists across datasets and architectures, identifying a key attack difficulty. Most crucially, this work establishes that the binding constraint on adversarial attacks is no longer the duration of observed audio but the quality of what can be predicted from it.

## Impact Statement

This work presents methods for generating adversarial attacks against automatic speech recognition (ASR) systems. We acknowledge that such attacks carry a meaningful potential for harm. ASR systems increasingly serve as a primary interface through which people interact with AI, and demonstrating that their outputs can be systematically manipulated raises legitimate safety concerns. These concerns are particularly acute for communities that rely on audio communication over text-based modalities, as such users may have limited ability to independently verify ASR performance or detect adversarial interference.

Nevertheless, we fundamentally believe that conducting adversarial research is crucial to understanding the limitations in current systems. Identifying the risks associated with adversarial manipulation of ASR models requires first establishing what those risks concretely are: under what conditions attacks succeed, what architectural properties they exploit, and how their effectiveness transfers across models and domains. Without this understanding, the research community and downstream deployers of ASR technology operate under a false sense of security, in which vulnerabilities persist but remain unexamined. The absence of published attacks does not imply the absence of exploitable vulnerabilities; it implies only that those vulnerabilities are poorly characterised. Choosing not to study potential failure modes offers the appearance of robustness without its substance. By systematically exposing and analysing the conditions under which ASR systems can be reliably manipulated, we aim to provide the empirical foundation upon which more effective defences and more responsible deployment practices can be built.

## References

- [1] Nicholas Carlini and David Wagner. Audio adversarial examples: Targeted attacks on speech-to-text. In *IEEE Security and Privacy Workshops (SPW)*, 2018.
- [2] Raphael Olivier, Hadi Abdullah, and Bhiksha Raj. Watch what you pretrain for: Targeted, transferable adversarial examples on self-supervised speech recognition models. In *IEEE Conference on Secure and Trustworthy Machine Learning (SaTML)*, 2024.
- [3] Peng Cheng, Yuwei Wang, Peng Huang, Zhongjie Ba, Xiaodong Lin, Feng Lin, Li Lu, and Kui Ren. ALIF: Low-cost adversarial audio attacks on black-box speech platforms using linguistic features. In *Proceedings of the 2024 ACM SIGSAC Conference on Computer and Communications Security (CCS)*, 2024. doi: 10.1145/3658644.3670356.
- [4] Mia Chiquier, Chengzhi Mao, and Carl Vondrick. Real-time neural voice camouflage. In *International Conference on Learning Representations (ICLR)*, 2022.
- [5] Alexei Baevski, Henry Zhou, Abdelrahman Mohamed, and Michael Auli. wav2vec 2.0: A framework for self-supervised learning of speech representations. In *Advances in Neural Information Processing Systems (NeurIPS)*, 2020.
- [6] Yao Qin, Nicholas Carlini, Ian Goodfellow, Garrison Cottrell, and Colin Raffel. Imperceptible, robust, and targeted adversarial examples for automatic speech recognition. In *Proceedings of the 36th International Conference on Machine Learning (ICML)*, 2019.
- [7] Paarth Neekhara, Shehzeen Hussain, Prakhar Pandey, Shlomo Dubnov, Julian McAuley, and Farinaz Koushanfar. Universal adversarial perturbations for speech recognition systems. In *Interspeech*, pages 481–485, 2019.
- [8] Qibin Sun, Shun Chen, Yingbin Zhai, Yang Liu, and Zhisheng Zhong. CommanderUAP: Practical and transferable universal adversarial perturbations on ASR systems. *Cybersecurity*, 2024. doi: 10.1093/cybsec/tyae003.

- [9] Lea Schönherr, Katharina Kohls, Steffen Zeiler, Thorsten Holz, and Dorothea Kolossa. Adversarial attacks against automatic speech recognition systems via psychoacoustic hiding. In *Network and Distributed System Security Symposium (NDSS)*, 2019. doi: 10.14722/ndss.2019.23288.
- [10] Joseph Szurley and J. Zico Kolter. Perceptual based adversarial audio attacks. *arXiv preprint arXiv:1906.06355*, 2019.
- [11] Yuan Gong, Boyang Li, Christian Poellabauer, and Yiyu Shi. Real-time adversarial attacks. In *Proceedings of the 28th International Joint Conference on Artificial Intelligence (IJCAI)*, pages 4672–4680, 2019.
- [12] Alex Graves, Santiago Fernández, Faustino Gomez, and Jürgen Schmidhuber. Connectionist temporal classification: Labelling unsegmented sequence data with recurrent neural networks. In *Proceedings of the 23rd International Conference on Machine Learning (ICML)*, pages 369–376. ACM, 2006.
- [13] Andrew Jaegle, Felix Gimeno, Andrew Brock, Andrew Zisserman, Oriol Vinyals, and João Carreira. Perceiver: General perception with iterative attention. In Marina Meila and Tong Zhang, editors, *Proceedings of the 38th International Conference on Machine Learning*, volume 139 of *Proceedings of Machine Learning Research*, pages 4651–4664. PMLR, 2021.
- [14] Vassil Panayotov, Guoguo Chen, Daniel Povey, and Sanjeev Khudanpur. LibriSpeech: An ASR corpus based on public domain audio books. In *2015 IEEE International Conference on Acoustics, Speech and Signal Processing (ICASSP)*, pages 5206–5210, 2015. doi: 10.1109/ICASSP.2015.7178964.
- [15] Romain Ardila, Megan Branson, Kelly Davis, Michael Kohler, Josh Meyer, Reuben Henretty, Gabriel Morais, Lindsay Saunders, Francis Tyers, and Gregor Weber. Common Voice: A massively-multilingual speech corpus. In *Proceedings of the 12th Language Resources and Evaluation Conference (LREC)*, pages 4218–4222, Marseille, France, 2020. URL <https://commonvoice.mozilla.org>.
- [16] Wei-Ning Hsu, Benjamin Bolte, Yao-Hung Hubert Tsai, Kushal Lakhotia, Ruslan Salakhutdinov, and Abdelrahman Mohamed. HuBERT: Self-supervised speech representation learning by masked prediction of hidden units. *IEEE/ACM Transactions on Audio, Speech, and Language Processing*, 29:3451–3460, 2021. doi: 10.1109/TASLP.2021.3122291.
- [17] Alec Radford, Jong Wook Kim, Tao Xu, Greg Brockman, Christine McLeavey, and Ilya Sutskever. Robust speech recognition via large-scale weak supervision. In *Proceedings of the 40th International Conference on Machine Learning (ICML)*, pages 28448–28493. PMLR, 2023.
- [18] Abhimanyu Dubey, Abhinav Jauhri, Abhinav Pandey, Abhishek Kadian, Ahmad Al-Dahle, Aiesha Letman, Akhil Mathur, Alan Schelten, Amy Yang, Angela Fan, et al. The Llama 3 herd of models. *arXiv preprint arXiv:2407.21783*, 2024.
- [19] Sajjad Abdoli, Luiz G. Hafemann, Jerome Rony, Ismail Ben Ayed, Patrick Cardinal, and Alessandro L. Koerich. Universal adversarial audio perturbations. *arXiv preprint arXiv:1908.03173*, 2019.
- [20] Aleksander Madry, Aleksandar Makelov, Ludwig Schmidt, Dimitris Tsipras, and Adrian Vladu. Towards deep learning models resistant to adversarial attacks. In *International Conference on Learning Representations (ICLR)*, 2018.
- [21] Jee-weon Jung, Hee-Soo Heo, Ju-ho Kim, Hye-jin Shim, and Ha-Jin Yu. RawNet: Advanced end-to-end deep neural network using raw waveforms for text-independent speaker verification. In *Interspeech*, pages 1268–1272, 2019. doi: 10.21437/Interspeech.2019-1982.
- [22] William Chan, Navdeep Jaitly, Quoc V. Le, and Oriol Vinyals. Listen, Attend and Spell: A neural network for large vocabulary conversational speech recognition. In *IEEE International Conference on Acoustics, Speech and Signal Processing (ICASSP)*. IEEE, 2016.

- [23] Shehzeen Hussain, Paarth Neekhara, Shlomo Dubnov, Julian McAuley, and Farinaz Koushanfar. WaveGuard: Understanding and mitigating audio adversarial examples. In *30th USENIX Security Symposium (USENIX Security 21)*, pages 2273–2290. USENIX Association, 2021.
- [24] Hiromu Yakura and Jun Sakuma. Robust audio adversarial example for a physical attack. In *Proceedings of the Twenty-Seventh International Joint Conference on Artificial Intelligence (IJCAI)*, 2018.
- [25] Xuejing Yuan, Yuxuan Chen, Yue Zhao, Yunhui Long, Xiaokang Liu, Kai Chen, Shengzhi Zhang, Heqing Huang, Xiaofeng Wang, and Carl A. Gunter. CommanderSong: A systematic approach for practical adversarial voice recognition. In *Proceedings of the 27th USENIX Security Symposium (USENIX Security 2018)*, pages 49–64. USENIX Association, 2018.
- [26] Yonghong Zong, Xiyang Zhang, Peiyu Hou, and Bo Wang. Targeted universal adversarial perturbations for automatic speech recognition. In *Information Security Conference (ISC)*, volume 13118 of *Lecture Notes in Computer Science*, 2021.
- [27] Raphael Olivier, Hadi Abdullah, and Bhiksha Raj. Transferable adversarial perturbations between self-supervised speech recognition models. In *ICML 2023 Workshop on New Frontiers in Adversarial Machine Learning (AdvML-Frontiers)*, 2023.
- [28] Abhishek Raina and Mark Gales. Controlling Whisper: Universal acoustic attacks on speech foundation models. *arXiv preprint arXiv:2404.01234*, 2024.
- [29] Dario Amodei, Sundaram Ananthanarayanan, Rishita Anubhai, Jing Bai, Eric Battenberg, Carl Case, Jared Casper, Bryan Catanzaro, Qiang Cheng, Guilin Chen, et al. Deep Speech 2: End-to-end speech recognition in English and Mandarin. In *Proceedings of the 33rd International Conference on Machine Learning (ICML)*, pages 173–182, 2016.
- [30] Linyang Li, Ruotian Ma, Qipeng Guo, Xiangyang Xue, and Xipeng Qiu. BERT-ATTACK: Adversarial attack against BERT using BERT. In *Proceedings of the 2020 Conference on Empirical Methods in Natural Language Processing (EMNLP)*, pages 6193–6202, 2020.
- [31] Patrick Chao, Alexander Robey, Edgar Dobriban, Hamed Hassani, George J. Pappas, and Eric Wong. Jailbreaking Black Box Large Language Models in Twenty Queries. *arXiv preprint arXiv:2310.08419*, 2023.
- [32] Lianmin Zheng, Wei-Lin Chiang, Ying Sheng, Siyuan Zhuang, Zhanghao Wu, Yonghao Zhuang, Zi Lin, Zhuohan Li, Dacheng Li, Eric Xing, et al. Judging LLM-as-a-judge with MT-bench and Chatbot Arena. In *Advances in Neural Information Processing Systems (NeurIPS)*, 2023.
- [33] Peiyi Wang, Lei Li, Liang Chen, Dawei Zhu, Binghuai Lin, Yunbo Cao, Qi Liu, Tianyu Liu, and Zhifang Sui. Large Language Models are not Fair Evaluators. *arXiv preprint arXiv:2305.17926*, 2023.
- [34] Bo Li, Shuo-yiin Chang, Tara N Sainath, Ruoming Pang, Yanzhang He, Trevor Strohman, and Yonghui Wu. Towards fast and accurate streaming end-to-end ASR. In *IEEE International Conference on Acoustics, Speech and Signal Processing (ICASSP)*, pages 6069–6073, 2020.
- [35] Hadi Abdullah, Muhammad Sajidur Rahman, Christian Peeters, Cassidy Gibson, Washington Garcia, Vincent Bindschaedler, Thomas Shrimpton, and Patrick Traynor. Beyond  $l_p$  clipping: Equalization-based psychoacoustic attacks against ASRs. In *Asian Conference on Machine Learning (ACML)*, volume 157 of *Proceedings of Machine Learning Research*, 2021.

## A Training and Architectural Details

**Training Procedure.** The generator (approximately 7.3M parameters) is trained for 4 epochs with Adam (learning rate  $1.5 \times 10^{-4}$ ,  $\beta_1 = 0.9$ ,  $\beta_2 = 0.999$ ) and an exponential learning rate schedule ( $\gamma = 0.99$ ), decayed once per epoch. No gradient clipping is applied. Training uses a batch size of 4 on a single NVIDIA A100 80 GB GPU (or H100 80 GB for AO runs), with a fixed random seed for reproducibility. Each SG training run (4 epochs) required approximately 15.5 A100 GPU-hours; GT

---

**Algorithm 2 SCALETOSNR: Perturbation amplitude normalization.**

---

**Require:** Raw perturbation  $\tilde{\delta} \in \mathbb{R}^N$ , injection-window signal  $x_* \in \mathbb{R}^N$ , target SNR  $\text{SNR}_{\text{tgt}}$  (dB)

**Ensure:** Constrained perturbation  $\delta$  satisfying  $\text{SNR}(x_*, \delta) = \text{SNR}_{\text{tgt}}$

- 1:  $\sigma_s \leftarrow \text{RMS}(x_*) = \sqrt{\frac{1}{N} \sum_{n=1}^N x_*[n]^2}$  ▷ Signal energy
  - 2:  $\sigma_{\text{tgt}} \leftarrow \sigma_s / 10^{\text{SNR}_{\text{tgt}}/20}$  ▷ Target noise RMS
  - 3:  $\sigma_{\tilde{\delta}} \leftarrow \text{RMS}(\tilde{\delta})$  ▷ Current perturbation energy
  - 4:  $\delta \leftarrow (\sigma_{\text{tgt}} / \sigma_{\tilde{\delta}}) \tilde{\delta}$  ▷ Uniform rescaling
  - 5: **return**  $\delta$
- 

and AO ablations required approximately 3.2 and 1.4 GPU-hours per run, respectively. Across the full  $(t_p, \tau)$  grid and both corpora, all reported experiments consumed approximately 500 GPU-hours. The SNR constraint is enforced by rescaling the generator output to the target noise RMS prior to injection; empirical SNR measured on the injected waveform matches the nominal value to within 0.15 dB throughout training. The final checkpoint after 4 epochs is used for evaluation. The same training procedure applies to the AO ablation and the GT upper bound (Section 4.2), differing only in the content of the text channel.

**Perturbation Scaling.** Algorithm 2 details the SCALETOSNR operator invoked at Line 6 of Algorithm 1. The operation applies a single scalar multiplication that modulates only the amplitude of the raw generator output  $\tilde{\delta}$ ; the waveform shape, which encodes the adversarial content, is produced entirely from causal, prefix-derived inputs by  $G_\theta$  (Algorithm 1, Line 5). Because the scaling factor is computed under `torch.no_grad`, no gradient signal from the target window  $x_*$  reaches the generator during training.

Since the scaling factor depends on  $\text{RMS}(x_*)$ , a natural question is whether this introduces a non-causal dependency at inference time. In a deployment setting the attacker controls the injection gain directly, for instance by calibrating loudspeaker volume or setting a digital mixing coefficient, and therefore does not need to compute the exact RMS of future speech in real time. This observation applies to any causal adversarial audio method: the energy of the yet-unobserved signal is never available at injection time, so every real-time attack must either estimate it or sidestep it through gain calibration. The causal information barrier of Section 2 governs the semantic content of the perturbation; amplitude scaling requires only a scalar energy estimate that can be derived causally with negligible loss of constraint precision. Empirically, speech energy is sufficiently stationary that a causal RMS estimate derived from the observed prefix shifts the effective SNR by only 1.3 dB at the median (mean 1.6 dB; 90th percentile 3.4 dB),<sup>1</sup> a margin well within the tolerance of practical imperceptibility budgets. We follow the standard convention in adversarial audio evaluation (1; 6; 9) and use the exact target-window energy, which ensures that constraint compliance is measured precisely rather than confounded by estimation noise.

**Design Choices.** The victim model (Wav2Vec 2.0 base, CTC-finetuned) is chosen as a widely benchmarked self-supervised ASR system representative of the CTC family; cross-architecture generality is tested separately in Section 4.5. The language model (Llama 3 8B, 8-bit quantized) balances forecast quality against inference latency within the streaming budget. The 15-token forecast horizon reflects the median token count of a 3.0 s speech segment in LibriSpeech; generating beyond this yields diminishing returns as excess tokens fall outside the target window. The 20 dB SNR constraint follows the perturbation budget standard in prior imperceptible audio attacks (1; 6; 9). The 3.0 s target window is set to match typical ASR chunk sizes in streaming deployments. Ablations comparing the primary generator architecture against three alternative fusion strategies are reported in Appendix E.

**Text Tokenization Pipeline.** The language model  $L$  (Llama 3 8B) operates over its native BPE vocabulary and produces up to 15 subword continuation tokens per prefix transcript  $y_p$ . These tokens are decoded back into a raw string, concatenated with the prefix transcript, and then re-tokenized at the character level using the victim model’s CTC alphabet (26 uppercase letters, apostrophe, and

---

<sup>1</sup>Measured over 1,263 LibriSpeech test utterances using equal-length adjacent windows of 3.0 s with no delay ( $\tau = 0$ ).

word-boundary marker, giving a vocabulary of 29 symbols). The resulting character indices are the input to the generator’s text embedding layer (labeled “Char embedding” in Figure 3). The 15-token horizon therefore refers to the LLM’s generation budget, not to the dimensionality of the generator’s text input; the character sequence seen by  $G_\theta$  is typically longer than 15 symbols, since each BPE token may decode to multiple characters.

## B Baseline Implementation Details

This appendix expands on the baselines summarized in Section 4.2.

**White Noise.** Gaussian noise is sampled at the input sample rate, applied over the same temporal extent as adversarial perturbations, and rescaled per utterance to enforce the SNR budget used by Semantic Gambit. No optimization is performed.

**Acoustic-Only Variants (AO and AO\*).** AO uses the same generator architecture, training procedure, and hyperparameters as Semantic Gambit but with the text channel zeroed: both the prefix transcription and the LLM continuation are replaced with zero vectors at the input to Stage 1, so the generator conditions only on the audio stream. No other modifications are made.

AO\* replicates the convolutional encoder-decoder of Chiquier et al. (4), mapping past spectral features to future adversarial waveforms without any text input. Two adaptations are required for comparison under our threat model: the perturbation budget is enforced via SNR rather than the original  $\ell_\infty$  constraint, and the attack target is redirected to the Wav2Vec 2.0 victim used throughout this work. All other architectural details follow the original implementation. AO\* is trained for 4 epochs with Adam (learning rate  $1.5 \times 10^{-4}$ ) and an exponential schedule ( $\gamma = 0.99$ ); no gradient clipping is applied, following the original implementation. Together, AO\*  $\rightarrow$  AO  $\rightarrow$  SG decomposes improvement over Chiquier et al. into an architectural component (AO\*  $\rightarrow$  AO, information held constant) and an informational component (AO  $\rightarrow$  SG, architecture held constant).

**Universal Adversarial Perturbation.** A single perturbation vector of fixed length is optimized via projected gradient ascent on CTC loss across the LibriSpeech training set. At inference, the vector is tiled to match the target utterance length and rescaled per sample to enforce the SNR constraint. Training uses Adam with a learning rate of  $5 \times 10^{-3}$  for 10 epochs; no learning rate schedule or gradient clipping is applied.

**Ground-Truth Upper Bound (GT).** The ground-truth forecast  $\tilde{y}_*^{\text{GT}}$  is obtained by passing the clean target window  $x_*$  through the victim ASR model directly, rather than via forced alignment of the reference transcript. This avoids alignment artifacts and ensures the oracle reflects exactly what the victim would output absent any attack. To match SG’s information budget, GT forecasts are truncated to at most 15 tokens using the Llama 3 tokenizer, ensuring the only difference between GT and SG is prediction accuracy rather than token count (denoted with the suffix `_tok15`). All other training hyperparameters (Adam, learning rate  $1.5 \times 10^{-4}$ , exponential schedule  $\gamma = 0.99$ , 4 epochs) follow Semantic Gambit.

**Projected Gradient Descent (PGD).** We use the standard PGD attack of Madry et al. (20) with 40 iteration steps and step size  $\alpha = 0.2 \varepsilon$ , where  $\varepsilon$  is the RMS bound implied by the 20 dB SNR constraint, following Chiquier et al. (4). Concretely, the per-utterance perturbation budget is

$$\varepsilon = \|x_*\|_2 \cdot 10^{-\text{SNR}_{\text{dB}}/20}, \quad (5)$$

and the perturbation is updated by

$$\delta^{(t+1)} = \Pi_{\mathcal{B}_\varepsilon} \left( \delta^{(t)} + \alpha \frac{\nabla_\delta \mathcal{L}_{\text{CTC}}(M(\tilde{x}^{(t)}), y^{\text{gt}})}{\|\nabla_\delta \mathcal{L}_{\text{CTC}}\|_2} \right), \quad (6)$$

where  $\tilde{x}^{(t)}$  denotes the full utterance  $x$  with the target segment replaced by  $x_* + \delta^{(t)}$ ,  $\Pi_{\mathcal{B}_\varepsilon}$  projects onto  $\{\delta : \|\delta\|_2 \leq \varepsilon\}$ ,  $M$  is the victim CTC model, and  $y^{\text{gt}}$  is the full length ground-truth transcription. Because PGD is an untargeted attack that maximizes the CTC loss with respect to the ground-truth transcription, the update follows the gradient (ascent) rather than negating it. PGD has non-causal

Table 3: **Sentence-level mean WER (%)** with 95% confidence intervals on LibriSpeech under a 20 dB SNR budget. CIs use the Gaussian approximation  $\bar{x} \pm 1.96 (\text{std}/\sqrt{n})$ . Best attack per row in **bold**. Sample size  $n$  varies (859 to 1850) with the prefix, target, and delay window length.

Prefix	Delay	SG (Ours)		AO		AO*	
		Mean	95% CI	Mean	95% CI	Mean	95% CI
1.0	0.0	<b>49.6</b>	[47.3, 51.9]	21.0	[19.9, 22.2]	16.4	[15.6, 17.3]
	0.5	21.9	[20.7, 23.0]	<b>25.8</b>	[24.5, 27.0]	10.5	[9.9, 11.2]
	1.0	<b>23.7</b>	[22.6, 24.8]	18.5	[17.6, 19.5]	6.4	[6.0, 6.9]
2.0	0.0	<b>41.9</b>	[39.9, 43.8]	15.9	[15.1, 16.8]	2.3	[2.1, 2.5]
	0.5	<b>25.7</b>	[24.2, 27.2]	17.3	[16.4, 18.1]	5.1	[4.8, 5.5]
	1.0	<b>23.4</b>	[22.1, 24.6]	16.5	[15.5, 17.4]	3.5	[3.2, 3.8]
3.0	0.0	<b>28.0</b>	[26.4, 29.6]	17.9	[16.9, 18.9]	4.7	[4.4, 5.1]
	0.5	<b>25.4</b>	[23.9, 26.9]	23.3	[22.1, 24.4]	2.5	[2.3, 2.7]
	1.0	<b>13.2</b>	[12.4, 14.0]	13.0	[12.2, 13.7]	9.7	[9.1, 10.2]
4.0	0.0	<b>24.3</b>	[22.8, 25.8]	23.3	[22.0, 24.7]	6.5	[6.1, 6.9]
	0.5	<b>22.3</b>	[20.9, 23.8]	17.4	[16.4, 18.4]	5.4	[5.0, 5.8]
	1.0	<b>21.5</b>	[20.3, 22.7]	20.3	[19.2, 21.4]	9.8	[9.2, 10.3]

access to the complete utterance during optimization – the full waveform, including audio beyond the target window, is passed through  $M$  at every iteration – and so violates the streaming constraint of Section 2; it is included only as a reference ceiling.

### C Sentence-Level Results with Confidence Intervals

The corpus-level WER reported in Section 4.3 aggregates errors across all evaluation utterances and is appropriate for assessing overall attack efficacy on the test set as a whole. To complement this view, we report sentence-level mean WER with 95% confidence intervals (Table 3), which characterizes the distribution of attack effectiveness across individual utterances rather than the pooled error rate. Confidence intervals use the Gaussian approximation  $\bar{x} \pm 1.96 (\text{std}/\sqrt{n})$ , where  $n$  ranges from 859 to 1850 depending on the (prefix, delay) configuration. The variation in  $n$  reflects the streaming evaluation protocol: at longer prefix and delay combinations, fewer LibriSpeech utterances are long enough to admit a complete (prefix, delay, target) window of the required duration. The clean sentence-level mean WER is stable across configurations at 2.04% to 2.16%, within 0.2% of its corpus-level counterpart, and we omit it from the table.

**Statistical Robustness Across the Streaming Grid.** SG’s interval lies strictly above Chiquier et al.’s (AO\*) in every cell, so the improvement over the prior streaming baseline is uniform rather than concentrated in a few favourable configurations. Against the AO ablation, the geometry is more textured: SG’s interval sits cleanly above AO’s across the short-prefix, zero-delay regime where semantic forecasting is expected to contribute most, and the two methods converge toward statistical parity as prefix length and delay grow. This pattern empirically corroborates the information-hierarchy argument of Section 4.3, with the separation between methods greatest precisely where the acoustic channel alone is most impoverished. We note one departure at a 1.0 s prefix and 0.5 s delay, where AO exceeds SG under non-overlapping intervals; its position at the shortest prefix with non-zero delay suggests a specific interaction with the Perceiver latent bottleneck that warrants separate investigation. Chiquier et al.’s performance reinforces the information-hierarchy argument from a different angle: even a purpose-built streaming attack collapses to near-clean WER at the tightest configurations when restricted to acoustic information alone.

**Sentence- versus Corpus-Level Magnitudes.** The sentence-level means systematically exceed the corresponding corpus-level WER under attack, and the gap scales with attack strength. At SG’s strongest cell (prefix 1.0 s, delay 0.0 s), the sentence-level mean of 49.6% exceeds the corpus-level value of 35.6% by roughly 14%; at weaker configurations the gap compresses to a few percent; under

clean conditions, where there is no induced error to amplify, the two views agree to within 0.2%. The discrepancy is methodological. Corpus-level WER weights errors by total reference length, so longer utterances dominate the aggregate, whereas the sentence-level mean treats each utterance equally. Length-stratified analysis confirms the mechanism: at SG’s strongest cell, medium-length utterances (6 to 15 words,  $n=456$ ) reach a median attack WER of 93.3%, while long utterances (16 or more words,  $n=1392$ ) sit at 27.2%. The fixed 3.0 s target window covers a larger fraction of short transcripts, so even a modest number of induced errors translates into a high per-sentence WER, which the equal-weighted mean preserves but the length-weighted aggregate dilutes. We treat both views as complementary: corpus-level WER governs comparisons against the prior streaming literature, which reports the same aggregate, while sentence-level intervals support the per-configuration significance claims above.

## D Streaming Latency Decomposition

The injection delay  $\tau$  in Section 4.1 parameterizes the time between the attacker’s last observation and the start of the perturbation window. In a deployed system, this delay reflects the wall-clock cost of three sequential operations: (i) the victim ASR transcribing the observed prefix, (ii) the LLM generating a semantic forecast from that transcript, and (iii) the generator producing the adversarial waveform. We measure each component independently and summarise the results in Table 4.

**Victim ASR Transcription.** In a streaming deployment, victim inference runs concurrently with audio arrival: the encoder processes frames as they are spoken, so only the final chunk contributes additional delay beyond the prefix duration itself. For CTC-based victims this cost is minimal, since frame-synchronous decoding requires no right-context lookahead. Across all four prefix lengths, Wav2Vec 2.0 completes its forward pass in under 7 ms on average, with near-constant latency confirming that this reflects fixed per-call GPU overhead rather than scaling with input duration.

Table 4: Streaming latency decomposition across the full  $(t_p, \tau)$  grid (NVIDIA A100).

Component	Mean (ms)	Range (ms)	Share (%)
Victim ASR transcription	5.9	5.22–6.97	< 1
LLM forecast	654	562–725	> 99
Generator forward pass	3.3	2.56–4.10	< 1
Total pipeline	663	564–729	100

**LLM Forecasting.** The LLM forecast (Llama 3 8B, 8-bit quantized, generating up to 15 tokens) is the dominant cost, accounting for over 99% of the pipeline. Inference averages approximately 654 ms, ranging from 562 to 725 ms across the grid. The variation reflects prompt length: longer prefixes produce longer transcripts, yielding a longer LLM context window.

**Generator Forward Pass.** The generator averages 3.3 ms, ranging from 2.56 to 4.10 ms. Like victim inference, this cost scales mildly with prefix length due to the increased number of encoder frames, but remains negligible in all configurations.

**End-to-end Budget.** The full pipeline completes in 564 to 729 ms, comfortably within the  $\tau = 1.0$  s budget of our most relaxed configuration. Victim transcription and generator inference together contribute under 12 ms; the pipeline is bottlenecked entirely by the LLM forecast. This bottleneck is architectural rather than fundamental: replacing Llama 3 8B with a smaller or distilled language model, adopting speculative decoding, or moving to a dedicated inference backend would reduce LLM latency substantially without any change to the attack framework itself. The generator and victim ASR components already operate at latencies compatible with  $\tau = 0.0$  s deployment, meaning that improvements to LLM serving translate directly into tighter real-time budgets. These numbers also align with the latency tolerances of production streaming ASR systems, which typically operate with endpointing latencies of several hundred milliseconds to nearly one second (34), meaning that an attacker’s pipeline cost is comparable to delays already present in deployed systems. The  $\tau$  grid in our experiments conservatively tests delays up to 1.0 s, but the empirical measurements suggest that even

the  $\tau = 0.5$  s setting already provides a realistic margin for current hardware. Comparison against AO and AO\* is uninformative on this axis, since neither invokes a language model; the relevant claim is not that SG is faster than methods that pay no semantic cost, but that the cost it does pay is practically deployable.

## E Transformer Architecture Comparison

This appendix presents the full experimental comparison of four Transformer-based generator variants, all sharing identical front-end encoders and waveform decoder. The variants differ only in the intermediate fusion mechanism that compresses the multi-modal context into a fixed-size latent representation, enabling controlled attribution of performance differences to the fusion strategy alone.

All four variants share a common backbone: audio features and text tokens are first projected into a shared embedding space, then routed through a fusion module that produces a fixed-size latent summary, from which transposed convolutions decode the waveform perturbation  $\delta$ . The fusion module is built around a Perceiver (13), chosen because its learnable latent queries decouple decoder cost from input length, allowing the same architecture to handle variable-length audio and text without quadratic scaling. The variants differ in (i) whether a Stage 1 self-attention encoder precedes the Perceiver, (ii) how modalities are tagged via segment embeddings (2-way audio/text vs. 3-way audio/prefix/forecast), and (iii) whether audio and text share a joint softmax inside the Perceiver or are kept as separate streams with gated fusion.

### E.1 Variant Descriptions

Table 5: Summary of generator architecture variants. All Perceiver modules use 16 latent queries and 4 layers. “3-way” denotes segment embeddings for audio, prefix text, and forecast text; “2-way” merges both into a single text segment.

Variant	Stage 1	Stage 2	Tests	Params
Var. A	None	Joint softmax, 2-way	3-way segments + Stage 1	~5.7M
Var. B	None	Joint softmax, 3-way	Stage 1 self-attention	~5.7M
Var. C	None	Gated dual cross-attn	Separated modality streams	~7.5M
SG	2-layer self-attn	Joint softmax, 3-way	<i>Best performing</i>	~7.3M

**Variant A – Perceiver Only.** Audio and text tokens are concatenated with two type embeddings and fused exclusively through a 4-layer Perceiver cross-attention module. The two modalities interact only through the query bottleneck.

**Variant B – Perceiver with 3-way Segment Embeddings.** Identical to Variant A except that text tokens receive per-position segment embeddings distinguishing prefix text (grounded in observed audio) from forecast text (LLM-predicted). Comparing Variant B with SG isolates the contribution of Stage 1, since both share the same segment embedding scheme.

**Variant C – Gated Dual Cross-Attention.** Audio and text are kept as separate streams throughout. At each Perceiver layer, latent queries independently cross-attend to audio and text through separate attention heads, then a learned sigmoid gate combines the outputs per query. Each modality has its own softmax normalization, preventing mutual dilution.

**SG – Multi-Modal Self-Attention + Perceiver.** The full two-stage architecture. Stage 1 consists of 2 TransformerEncoder layers enabling direct bidirectional attention between audio frames and text tokens. Stage 2 is a standard 4-layer Perceiver with 3-way segment embeddings. The additional self-attention layers add ~1.6M parameters over Variant A/Variant B.

### E.2 Results and Analysis

At zero delay, SG achieves the highest corpus-level WER at every prefix length, with a substantial margin at short prefixes (35.63% vs the next-best 28.31% from Variant C at prefix of 1.0 s). The

Table 6: Architecture comparison (Target: 3.0 s): **Corpus-level WER (%)** against Wav2Vec 2.0 Large under **20 dB SNR**.

Prefix (s)	Delay (s)	Clean	Architecture Variants			SG
			Var. A	Var. B	Var. C	
1.0	0.0	2.05	21.84	25.18	28.31	<b>35.63</b>
	0.5	2.05	25.85	23.86	20.62	19.31
	1.0	2.02	17.27	17.79	21.45	18.89
2.0	0.0	2.02	21.20	20.82	11.69	<b>32.72</b>
	0.5	2.01	21.97	20.86	14.12	20.32
	1.0	2.03	16.62	28.28	14.70	18.95
3.0	0.0	2.03	14.96	16.63	16.44	<b>22.69</b>
	0.5	2.02	11.48	24.13	14.00	21.17
	1.0	2.01	20.91	12.35	21.47	11.32
4.0	0.0	2.01	15.12	17.57	15.24	<b>20.57</b>
	0.5	1.98	24.66	18.96	13.03	19.12
	1.0	1.97	12.84	11.94	15.38	18.68

Table 7: Architecture comparison (Target: 3.0 s): **Sentence-level mean WER (%)** against Wav2Vec 2.0 Large under **20 dB SNR**.

Prefix (s)	Delay (s)	Clean	Architecture Variants			SG
			Var. A	Var. B	Var. C	
1.0	0.0	2.16	30.46	34.58	38.68	<b>49.60</b>
	0.5	2.15	34.68	32.19	27.71	24.68
	1.0	2.08	21.98	22.36	27.61	23.72
2.0	0.0	2.08	27.30	26.38	14.92	<b>41.86</b>
	0.5	2.09	27.17	25.72	17.38	25.69
	1.0	2.12	20.08	35.11	17.89	23.35
3.0	0.0	2.12	18.33	20.39	19.87	<b>28.01</b>
	0.5	2.12	13.59	28.81	16.83	25.44
	1.0	2.10	24.55	14.25	25.55	13.18
4.0	0.0	2.10	17.67	20.67	17.79	<b>24.33</b>
	0.5	2.06	28.82	22.04	16.26	22.33
	1.0	2.04	14.60	13.55	17.74	21.50

advantage narrows at longer prefixes (20.57% vs 17.57% from Variant B at prefix of 4.0 s), consistent with the general observation that all text-containing architectures converge toward similar performance as prefix length increases.

**Contribution of Stage 1 (Variant B vs SG).** Comparing Variant B and SG isolates the effect of the 2-layer self-attention encoder. At zero delay, SG consistently outperforms Variant B: by 10.45% at prefix of 1.0 s, 11.90% at prefix of 2.0 s, 6.06% at prefix of 3.0 s, and 3.00% at prefix of 4.0 s. The diminishing gap at longer prefixes suggests that Stage 1’s cross-modal attention is most valuable when the context is compact enough for the model to learn meaningful audio–text correspondences.

**Value of Segment Embeddings (Variant A vs Variant B).** Variant A and Variant B differ only in their segment embedding scheme: 2-way vs 3-way. At zero delay, Variant B outperforms Variant A at three of four prefix lengths (by 3.34% at prefix of 1.0 s, 1.67% at prefix of 3.0 s, and 2.45% at prefix of 4.0 s), while Variant A holds a marginal edge at prefix of 2.0 s (21.20% vs 20.82%). The benefit of distinguishing prefix transcription from LLM forecast is therefore modest but broadly consistent.

**Separate Modality Streams (Variant C vs SG).** Variant C’s gated dual cross-attention underperforms SG at zero delay across all prefix lengths (28.31% vs 35.63% at prefix of 1.0 s; 15.24% vs 20.57% at prefix of 4.0 s). This result is particularly informative in light of the earlier SG-Causal finding. In Phase 1, we attributed SG-Causal’s under-performance partly to a capacity bottleneck: its lightweight linear fusion and sparse parameter distribution prevented the separate-encoding design

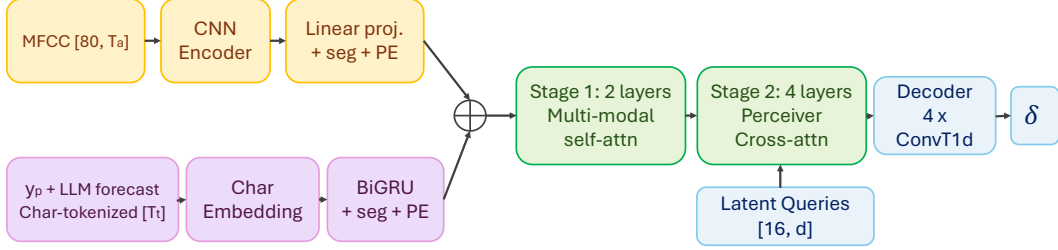


Figure 3: Architecture of the SG generator. Audio features (MFCC) and text tokens (prefix transcript + LLM forecast, character-tokenized; see Appendix A) are encoded separately, annotated with modality and role segment embeddings, and fused through two stages: joint self-attention over the concatenated sequence (Stage 1, 2 layers), followed by Perceiver cross-attention from 16 learnable latent queries (Stage 2, 4 layers). The resulting latent summary is decoded into a waveform perturbation  $\delta$  via transposed convolutions. All components are trained jointly.

from exploiting the explicit causal boundary. Variant C tests whether a more powerful separate-stream mechanism—gated dual cross-attention with dedicated per-modality softmax normalization and  $\sim 7.5M$  parameters, exceeding even SG’s  $\sim 7.3M$ —can recover the lost ground. The fact that it cannot suggests that the disadvantage of separate modality streams is not purely a capacity limitation but reflects a more fundamental issue: keeping audio and text in isolated pathways, even with learned gating, prevents the fine-grained token-level interactions that joint self-attention enables in SG. The separate-stream design may preserve cleaner per-modality representations, but at the cost of the direct audio–text alignment that appears critical for generating effective perturbations.

However, Variant C shows more competitive results at a delay of 1.0 s (e.g. 21.45% and 21.47% at prefix of 1.0 s and 3.0 s), suggesting that the separate-stream design may have advantages in the delayed-injection scenario where temporal alignment between modalities is less direct. More broadly, the configuration-dependent instability observed at non-zero delays persists across all four Transformer variants—mirroring the same pattern documented for the earlier SG-Combined and baseline architectures, and further reinforcing the interpretation that this variance is a systematic property of adversarial CTC optimization rather than an artifact of any particular fusion design.

## F Investigating the Prefix Length Effect

The corpus-level WER results in the main paper (Table 1) show that the WER of all text-conditioned attacks decreases as the observed prefix grows longer at zero delay, while the acoustic-only ablation remains roughly stable. The same pattern holds across every text-containing generator variant we evaluated: Variant A, Variant B, SG, and Variant C all decline monotonically from a 1.0 s prefix to a 4.0 s prefix (Appendix E, Tables 6–7). This appendix documents the investigation behind the main paper’s claim that the decline reflects an intrinsic diminishing of the text channel’s marginal value. We test three hypotheses, conduct attention-map analysis, run two architectural interventions, and rule out training-budget confounds, concluding that the effect cannot be attributed to any specific architectural design choice and is most parsimoniously explained as a property of the prediction problem itself.

### F.1 The Observation

The main paper attributes the prefix-length decline to two compounding mechanisms: a victim-side effect, in which longer prefixes give the ASR a cleaner anchor for decoding, and a text-channel effect specific to text-conditioned attacks. The decline is broad – PGD, AO\*, GT, and SG all decline with prefix length – but its magnitude varies across methods, and the contrast that frames this appendix’s investigation is the gap between text-conditioned attacks and the acoustic-only ablation. If the victim-side effect were the dominant mechanism, the acoustic-only ablation should decline at a comparable rate to the text-conditioned variants. It does not (corpus-level WER of 15.15%, 12.58%, 14.82%, 19.85% across the four prefix lengths), suggesting that an additional, text-channel-specific mechanism is contributing to the steeper declines observed in Variant A, Variant B, SG, and Variant C. Quantitatively, SG’s advantage over the acoustic-only ablation collapses from +20.48% at a prefix

of 1.0 s to just +0.72% at a prefix of 4.0 s. The text channel’s contribution to attack effectiveness diminishes sharply as prefix length grows, and a similar collapse is observed across Variant A, Variant B, SG, and Variant C, suggesting the effect is not tied to any particular fusion mechanism.

## F.2 Hypotheses and Interventions

Three hypotheses were formulated and tested.

**Hypothesis 1: Victim-Side CTC Anchor Effect.** A longer clean prefix provides the victim ASR with more correctly-aligned frames, creating a stronger alignment anchor that helps resist corruption in the target window. *Evidence:* The GT upper bound declines from 23.53% to 12.44% across prefix lengths, confirming that the attack problem does become harder. *Limitation:* This cannot be the sole explanation because the acoustic-only ablation does not decline – the victim-side effect should apply equally to all attack variants.

**Hypothesis 2: Perceiver Bottleneck.** The fixed 16 latent queries may be insufficient to compress the growing multi-modal context (108 tokens at prefix = 1.0 s vs 168 at prefix = 4.0 s). *Attention map analysis* confirmed that attention entropy saturates at longer prefixes: peak weights collapse from 0.05–0.20 at prefix = 1.0 s to 0.008–0.018 at prefix = 4.0 s, and Shannon entropy approaches the theoretical maximum (see Figures 5 and 6 in Subsection F.4). *Interventions tested:*

- **Increased query count** ( $n_{\text{latent}} = 32$ ): Performance degraded across all configurations (e.g. 19.70% vs 35.63% at prefix = 1.0 s). However, this result is confounded by the waveform decoder’s architectural coupling to 16 temporal frames – doubling the query count disrupts the decoder’s transposed-convolution chain, making the comparison inconclusive.
- **Separate-softmax cross-attention:** Audio and text tokens receive independent softmax normalization with a learned gate combining the outputs. Performance degraded at *all* prefix lengths, including short prefixes where entropy saturation was not observed (24.28% vs 35.63% at prefix = 1.0 s). This demonstrates that the joint softmax is actively beneficial, not a bottleneck.

*Conclusion:* The entropy saturation observed in the attention analysis is a real correlational phenomenon but is not causally responsible for the WER decline. The joint softmax and fixed query count are well-functioning components of the architecture.

**Hypothesis 3: Diminishing Marginal Value of Text.** The text channel’s informational value for generating adversarial perturbations may inherently diminish at longer prefixes. *Evidence:* The text channel’s contribution (SG minus acoustic-only) collapses from ~20% to <1%. The acoustic-only ablation, which processes only audio tokens (13–51 tokens across prefix lengths) and never faces the growing text context, remains stable. Since the decline is universal across architectures with fundamentally different fusion mechanisms (joint attention, separate streams, with/without Stage 1), it cannot be attributed to any particular design choice. *This is the explanation most consistent with the full body of evidence.*

## F.3 Training Convergence

One potential confound is that longer-prefix models, which process more context tokens per step, may be under-trained given the same training budget (4 epochs, ~28,500 steps). We rule this out by examining the final training CTC loss: at both prefix = 1.0 s and prefix = 4.0 s, the loss in the final 1,500 steps oscillates in the same range (approximately 0.2–2.5) with comparable gradient norms and identical learning rates. Neither model shows a systematic downward trend, indicating incomplete convergence.

## F.4 Attention Map Analysis

To understand the internal dynamics of SG under varying prefix configurations, we extracted attention weights from all four Perceiver decoder layers by patching PyTorch’s `MultiheadAttention` modules to capture per-head matrices during evaluation. For each prefix configuration (1.0–4.0 s, delay = 0.0 s), we analyzed 20 batches (~60 samples).

**Modality Balance.** The audio attention fraction remains stable at 30–40% across all prefix configurations (Table 8, Figure 4). The Pearson correlation with WER is weak ( $r = -0.29$ ), ruling out the hypothesis that audio tokens progressively dominate the softmax at longer prefixes. The same picture holds at the per-query level: audio fractions fall in the 15–60% range at both prefix lengths, with no query attending exclusively to one modality and the aggregate balance broadly preserved.

Table 8: Mean audio attention fraction (%) in Stage 2 cross-attention by decoder layer (delay = 0.0 s, 20 dB SNR).

Prefix (s)	L0	L1	L2	L3	Avg
1.0	33.8	37.0	32.2	46.8	37.5
2.0	38.5	33.2	29.3	17.1	29.5
3.0	45.1	52.1	29.6	35.7	40.6
4.0	35.3	33.5	37.3	30.6	34.2

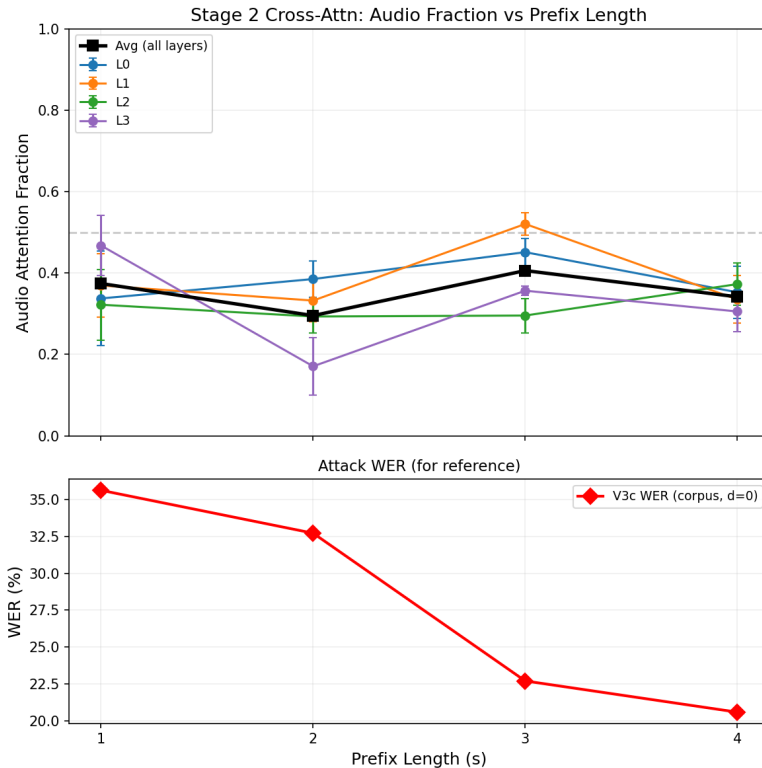


Figure 4: Audio attention fraction (top) and attack WER (bottom) vs prefix length. Despite the WER declining monotonically, the audio fraction remains stable at 30–40% ( $r = -0.29$ ).

**Peak Weight Collapse and Entropy Saturation.** While modality balance is broadly preserved, attention selectivity is not. Figure 5 shows a roughly  $10\times$  collapse in peak attention weight from prefix = 1.0 s (peaks of 0.15–0.35) to prefix = 4.0 s (peaks barely exceeding 0.02), plotted on a shared x-axis to make the magnitude directly comparable. Figure 6 quantifies this loss of selectivity using Shannon entropy: at prefix = 1.0 s (80 total tokens), query entropies sit in the 3.5–4.0 bit range against a theoretical maximum of 6.3 bits, leaving substantial headroom for selective attention; at prefix = 4.0 s (170 total tokens), entropies push to roughly 7.0 bits against a maximum of 7.4 bits, within 0.5 bits of saturation.

A notable observation is that at prefix = 4.0 s, the majority of queries’ peak positions shift to text tokens (orange bars in Figure 5), reversing the audio-leaning peak pattern visible at 1.0 s. However,

these “peaks” carry weights of only 0.015–0.020, barely 2–3 $\times$  above the uniform baseline of  $1/170 \approx 0.006$ , representing statistical fluctuation rather than genuine selective attention.

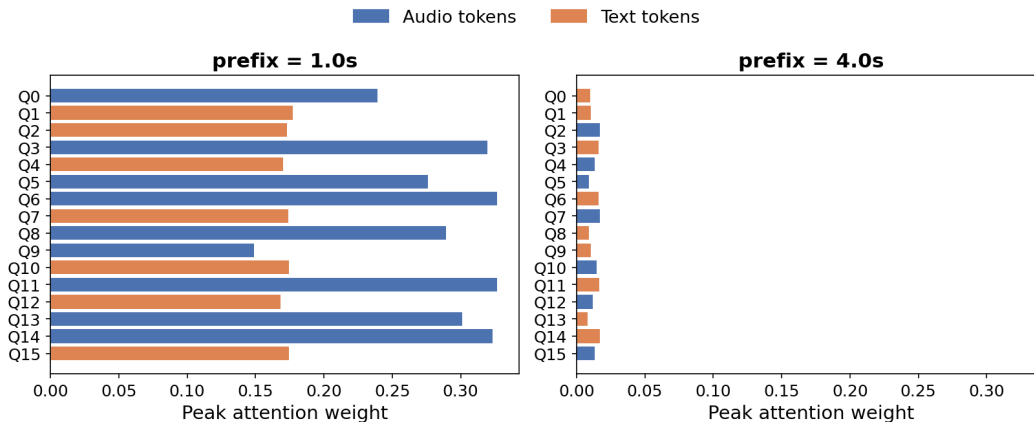


Figure 5: Per-query peak attention weight at the final Perceiver decoder layer, compared between prefix lengths of 1.0 s and 4.0 s (delay = 0.0 s, head-averaged, single representative example). Bar color encodes the modality of each query’s argmax position (blue represents audio, orange represents text). The x-axis is shared across columns to make the magnitude of the collapse directly visible.

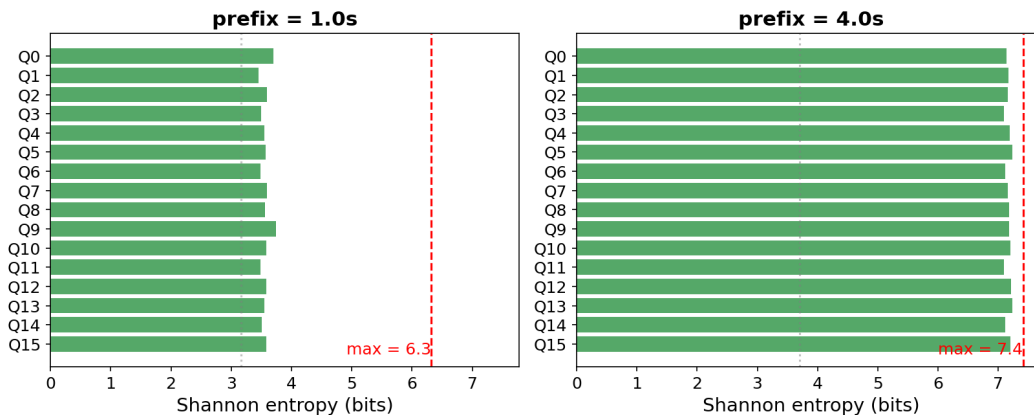


Figure 6: Per-query Shannon entropy of attention distributions at the final Perceiver decoder layer, compared between prefix lengths (delay = 0.0 s, head-averaged). Red dashed line marks the maximum possible entropy ( $\log_2 T$ ) for each prefix length; gray dotted line marks 50% of max. At 4.0 s, query entropies approach saturation, leaving the queries with no effective selective attention.

**Interpretation.** The three diagnostics paint a coherent picture of how SG’s attention adapts—and fails to adapt—to longer prefixes. Modality balance is preserved: the architecture continues to allocate roughly a third of its attention mass to audio at every prefix length, so the WER decline is not explained by either modality being squeezed out of the softmax. What does change is selectivity. The peak-weight collapse and the entropy saturation are two views of the same phenomenon: as the context grows from 80 to 170 tokens, the queries can no longer concentrate on a small set of informative positions, and the attention distribution flattens toward uniformity. The apparent shift of peak positions toward text tokens at 4.0 s is a consequence of this flattening rather than a meaningful preference, since the “peaks” themselves sit only 2–3 $\times$  above the uniform baseline.

Whether this selectivity loss is a *cause* of the WER decline or a *symptom* of it is the natural next question. The diagnostics alone cannot distinguish the two: a model that has learned to lean less on the text signal would also exhibit flattened attention, since there is less to attend to. We resolve this question in Section F.5 by directly intervening on the bottleneck (more queries, separated softmaxes), and find that neither intervention helps—an outcome inconsistent with the bottleneck-as-cause reading.

## F.5 Architectural Interventions

Table 9 summarizes the results of the two architectural interventions motivated by the attention analysis. Both are compared against the standard SG at delay = 0.0 s.

Table 9: Architectural interventions targeting the Perceiver bottleneck, compared against standard SG (delay = 0.0 s, 20 dB SNR). Both interventions degrade performance.

Prefix (s)	SG	32-query	Sep-softmax
1.0	<b>35.63</b>	19.70	24.28
2.0	<b>32.72</b>	13.75	19.39
3.0	<b>22.69</b>	19.79	16.64
4.0	<b>20.57</b>	21.28	14.65

The 32-query variant’s degradation is partially attributable to a decoder confound (see Appendix E). The sep-softmax variant’s degradation at *all* prefix lengths, including short prefixes where entropy saturation is absent, provides the strongest evidence that the joint softmax is an integral part of SG’s success rather than a bottleneck to be resolved.

## F.6 Summary

The prefix length effect is a robust empirical phenomenon that cannot be attributed to any specific architectural design choice, training insufficiency, or attention mechanism failure. The most parsimonious explanation consistent with all evidence is that the marginal value of semantic conditioning for adversarial perturbation generation diminishes as the prefix length increases. At short prefixes, the text channel provides substantial additional attack capability (+20% over acoustic-only); at long prefixes, this advantage is nearly eliminated. The acoustic-only ablation’s stability confirms that the decline is specifically tied to the text channel’s diminishing contribution rather than a general difficulty increase.

## G Cross-Dataset Transferability

This appendix provides the complete experimental results supporting Section 4.4. Section G.1 documents the Common Voice preparation pipeline and summarizes the key differences between the two datasets. Section G.2 details the matched-compute training configuration. Section G.3 reports the full  $2 \times 2 \times 4$  transferability matrix (two training datasets  $\times$  two evaluation datasets  $\times$  four prefix configurations). Section G.4 addresses the subset-matching confound introduced by prefix-dependent duration filters. Section G.5 reports length-stratified results. Section G.6 documents constraint compliance.

### G.1 Common Voice Preparation

Common Voice 25.0 English was obtained from the Mozilla Data Collective (87.84 GiB, 2.57M clips across train/dev/test splits). The official test split (16,398 clips) was retained in full. The train split (1,147,465 validated clips) was randomly sub-sampled to 250,000 clips. MP3 clips were decoded with librosa, resampled to 16 kHz mono, filtered to a minimum duration of 4.0 s (to accommodate our loosest prefix configuration, prefix 1.0 s plus target 3.0 s), and written as uncompressed WAV. Audio-decode failures affected 5.7% of clips and were dropped. Text transcripts were normalized to match LibriSpeech conventions: uppercased, punctuation stripped, whitespace collapsed, apostrophes retained. After preprocessing and downsampling, the effective training set contained 250,000 clips and the test set 13,606 clips passing the duration filter (longer-prefix configurations evaluate on smaller subsets; see Section G.4).

Table 10 summarizes the key differences between the two datasets. These differences make the cross-dataset experiment a stringent test of generalization: a generator trained on one distribution must produce perturbations that degrade the victim on audio with substantially different acoustic properties.

Table 10: Summary of dataset differences between LibriSpeech-100 and Common Voice 25.0 English.

	LibriSpeech-100	Common Voice
Speakers	~1,000	99,724
Accent coverage	US English (audiobook)	Global English
Recording conditions	Studio, read speech	Consumer mic, varied
Mean clip length	12.7 s	5.3 s
Training clips	28,539	250,000
Test clips (prefix 1.0 s)	1,850	13,606
Clean WER (W2V2)	≈2%	≈26%

## G.2 Training Configuration

Each prefix configuration (1.0 s, 2.0 s, 3.0 s, 4.0 s; delay 0 s, target 3 s) was trained for 28,500 gradient steps at batch size 4, learning rate  $1.5 \times 10^{-4}$ . This exactly matches the step budget used for the LS-100 experiments, yielding 114,000 clip-passes per run. The LS-100 pool (28,539 clips) is smaller than the CV subsample (250,000 clips), so LS training completes approximately 4 epochs while CV training completes approximately 0.45 epochs. We note that both regimes achieve attack saturation within budget ( $ASR@0.10 \geq 95\%$  in same-dataset evaluation for all prefix configurations), indicating that the compute-matched comparison is not confounded by sample exposure differences.

All other hyperparameters are identical to the main paper: SG generator with 16 latent queries, joint softmax, SNR 20 dB constraint,  $k = 15$  forecast tokens from Meta-Llama-3-8B. Each run consumed approximately 4 GPU-hours on an NVIDIA H100.

## G.3 Full Transferability Matrix

Table 11 reports all sixteen cells of the transferability matrix with evaluation-set sizes and clean WER baselines. Each row is one (train, eval, prefix) combination. Evaluation subsets decrease with prefix length due to the duration filter (min duration = prefix + target).

Table 11: Full cross-dataset transferability matrix across all four prefix configurations.  $N$  is the number of evaluation utterances whose duration exceeds the prefix length.  $\Delta WER$  is the median per-utterance WER increase in percentage points.  $ASR@_\tau$  is the fraction of utterances with  $\Delta WER \geq \tau$  (expressed as a ratio). Clean WER is constant within each (eval, prefix) pair and is reported once per group.

Train	Eval	Prefix	$N$	Clean WER	$\Delta WER$ (%)	$ASR@0.10$	$ASR@1.00$
LS	LS	1.0	1,850	2.05%	+33	76.5%	14.6%
		2.0	1,531	2.02%	+29	77.0%	8.4%
		3.0	1,263	2.03%	+19	64.3%	2.8%
		4.0	1,051	2.01%	+16	60.6%	1.5%
LS	CV	1.0	13,606	25.76%	+183	98.3%	85.5%
		2.0	10,826	26.06%	+182	97.8%	82.5%
		3.0	7,530	26.54%	+155	96.2%	74.3%
		4.0	4,697	27.39%	+158	94.0%	76.3%
CV	LS	1.0	1,850	2.05%	+18	61.2%	9.4%
		2.0	1,531	2.02%	+24	66.5%	9.5%
		3.0	1,263	2.03%	+17	63.2%	2.9%
		4.0	1,051	2.01%	+11	52.3%	0.1%
CV	CV	1.0	13,606	25.76%	+175	98.0%	80.9%
		2.0	10,826	26.06%	+192	98.1%	84.5%
		3.0	7,530	26.54%	+157	97.4%	79.7%
		4.0	4,697	27.39%	+94	95.0%	48.5%

Two observations beyond those in the main text. First, evaluation-set sizes shrink substantially with prefix length, so longer-prefix results are computed on a progressively smaller (and longer-utterance) subset; the implications of this subset dependence are discussed in Section G.4. Second, at the longest

prefix, the CV-trained generator shows a pronounced drop in attack effectiveness when evaluated on CV, while the LS-trained generator does not. This asymmetry points to a training-data bottleneck rather than an inherent limitation of the attack at longer prefixes: CV’s shorter mean clip length leaves few training examples that can accommodate a 4.0 s prefix alongside a full target window, starving the generator of viable training pairs. LS, with substantially longer recordings, retains enough usable clips to maintain attack strength. The pattern suggests that scaling to longer prefixes is primarily a data-coverage problem, and that a corpus with sufficient long-form audio should not exhibit the same degradation.

#### G.4 Subset-Matching Caveat

Each prefix configuration evaluates on the subset of the test set whose clips are at least (prefix + target) s long. Direct numerical comparison across prefix configurations therefore conflates attack effectiveness with evaluation-subset characteristics (e.g., longer clips may contain more syntactic context that the attack must disrupt).

We note that the qualitative ranking across prefixes is consistent with Section F’s LS-only results, where the same subset-dependence exists. For cross-dataset comparison at a fixed prefix (the primary claim of Section 4.4), the confound does not apply: both same-dataset and cross-dataset evaluations at a given prefix use identical subsets.

#### G.5 Length-Stratified Results

Does the attack affect short utterances differently from long ones? This matters for two reasons. First, short utterances mechanically inflate  $\Delta$ WER because WER normalizes by reference length—a handful of hallucinated tokens against a 3-word reference produces a  $\Delta$ WER several times larger than the same hallucination against a 20-word reference. ASR@0.10 sidesteps this inflation because it only asks whether the attack raised WER by at least 10 percentage points. Second, longer utterances give the victim more contextual information for partial recovery, so length-sensitivity reveals whether the attack succeeds by local corruption or by systematic transcript disruption.

We partition test utterances by reference-transcript word count (Short: 1–5 words; Medium: 6–15 words; Long: 16+ words) and report ASR@0.10 within each bin at prefix 2.0 s. We select this configuration because it avoids the extremes of the prefix range: prefix 1.0 s retains the largest evaluation subset and may overrepresent short CV clips, while prefix 4.0 s retains the smallest and skews toward longer utterances. Prefix 2.0 s provides a more balanced view of the length distribution across both datasets.

Table 12: Length-stratified attack success (ASR@0.10) at prefix 2.0 s. Cell values are the fraction of utterances where the attack raised WER by at least 10 percentage points. The Short bin is empty for LS evaluation because LS test-clean (audiobook narration) contains no clips with transcripts of fewer than six words.

Train	Eval	Short (1–5)	Medium (6–15)	Long (16+)
LS	LS	–	91.2% ( $n=194$ )	74.9% ( $n=1,337$ )
LS	CV	95.3% ( $n=383$ )	97.9% ( $n=10,189$ )	95.7% ( $n=254$ )
CV	LS	–	89.7% ( $n=194$ )	63.1% ( $n=1,337$ )
CV	CV	95.3% ( $n=383$ )	98.2% ( $n=10,189$ )	96.5% ( $n=254$ )

Two patterns emerge. On CV evaluation, attack success is near-universal across all length bins (95–98%): the victim’s 26% clean WER leaves so little baseline performance that even long utterances offer no recovery. On LS evaluation, success drops noticeably from Medium to Long bins—91.2% to 74.9% for LS to LS and 89.7% to 63.1% for CV to LS—indicating that a well-performing victim can use longer context to partially recover from the perturbation. This length-sensitivity is consistent with the victim-difficulty explanation discussed in Section 4.4: the attack’s apparent weakness on LS is bounded by how little room the victim has to degrade, and part of that remaining room is absorbed by contextual redundancy in longer utterances.

## G.6 Constraint Compliance

Table 13 documents empirical SNR and  $L_\infty$  perturbation magnitudes across all four matrix cells at prefix 2.0 s. Empirical SNR is tightly clustered around the 20 dB target in every condition, confirming that the generator respects the perturbation budget and that the effectiveness differences reported above are not driven by constraint violations.

Table 13: Empirical SNR (dB) and  $L_\infty$  perturbation magnitudes at prefix 2.0 s. Mean  $\pm$  standard deviation over the full evaluation set. Target SNR was 20 dB.

Train	Eval	SNR (dB)	$L_\infty$
LS	LS	20.03 $\pm$ 0.02	0.034 $\pm$ 0.011
LS	CV	20.08 $\pm$ 0.17	0.044 $\pm$ 0.035
CV	LS	20.03 $\pm$ 0.02	0.049 $\pm$ 0.016
CV	CV	20.08 $\pm$ 0.17	0.063 $\pm$ 0.049

## H Cross-Model Transferability

We assess whether adversarial perturbations crafted by our attack retain effectiveness when transcribed by an unseen victim ASR model. This is a strict black-box transfer setting: the generator is trained against one surrogate and never updated; at evaluation time we substitute only the model that produces the final transcription. The MFCC frontend, prefix transcription, LLM forecasting, and token encoding paths all remain aligned with the training-time surrogate, since these are part of the attack pipeline rather than the victim.

We evaluate three transfer scenarios spanning two architectural families. Within the CTC self-supervised family, we measure transfer in both directions of the W2V2 and HuBERT pair: (i) W2V2-trained generators transcribed by HuBERT-Large-LS960-ft (16), and (ii) HuBERT-trained generators transcribed by W2V2. To probe cross-family transfer, we additionally evaluate (iii) W2V2-trained generators transcribed by Whisper-small (17), an encoder-decoder seq2seq model trained with weak supervision on 680k hours of multilingual audio.

### H.1 Setup

For each (prefix, delay) configuration and each surrogate, we load the generator checkpoint trained against that surrogate, generate adversarial audio for the LibriSpeech test-clean split, and transcribe both clean and adversarial waveforms through the transfer victim. Empirical SNR is held at 20 dB across all runs (median 20.03 dB,  $\sigma < 0.03$  dB), confirming that the perturbation budget is preserved end-to-end. The number of evaluable utterances varies with the total audio length required (prefix + delay + target  $\leq T$ ), ranging from 1,850 utterances for the shortest configuration to 859 for the longest. Clean WER on each victim is approximately 2.0% across configurations.

We report corpus-level WER on the full utterance and target-window WER restricted to the perturbed segment, which more directly measures local attack efficacy. We additionally report the ASR@ $\tau$  family of attack-success metrics, defined as the fraction of utterances with  $\Delta\text{WER} \geq \tau$ .

### H.2 HuBERT-Surrogate In-Domain Effectiveness

We first establish that the HuBERT surrogate produces a viable in-domain attack across the full prefix $\times$ delay grid, mirroring the W2V2-surrogate baseline shown in Table 1.

The HuBERT-surrogate generator achieves attack WER between 12.7% and 27.2% across all 12 configurations, against a clean baseline of approximately 2.0%—a 6 to 14 times degradation. The strongest in-domain attack occurs at prefix is 1.0 s, delay is 0.5 s (27.18% corpus WER), with the strongest length-stratified effect on medium-length utterances of 6–15 words (median  $\Delta\text{WER}$  up to 69%). These numbers are roughly 70–80% of the corresponding W2V2-surrogate in-domain numbers in Table 1, indicating that HuBERT is a moderately harder surrogate to attack but a viable one nonetheless. This validates the HuBERT-surrogate generator as a meaningful basis for the cross-model transferability analysis that follows.

Table 14: In-domain attack WER (%) for the HuBERT-surrogate-trained generator evaluated on HuBERT-Large-LS960-ft. Clean WER on HuBERT is 2.00–2.06% across all configurations.

Prefix (s)	Delay 0.0 s	Delay 0.5 s	Delay 1.0 s
1.0	21.21	27.18	19.96
2.0	25.17	18.63	25.42
3.0	14.64	14.79	14.44
4.0	14.97	21.87	12.69

### H.3 Cross-Model Transferability

We now report cross-model transferability across the full prefix×delay grid in both directions of the W2V2 and HuBERT pair.

Table 15: Cross-model transfer attack WER (%) between W2V2 and HuBERT. Each cell shows the attack WER when the generator was trained against one surrogate and the victim is the other model: **W2V2** → **HuBERT** denotes a generator trained against W2V2 and evaluated against HuBERT-Large-LS960-ft, and **HuBERT** → **W2V2** denotes a generator trained against HuBERT and evaluated against W2V2. Clean WER on both victims is approximately 2.0% across configurations.

Prefix (s)	<b>W2V2</b> → <b>HuBERT</b>			<b>HuBERT</b> → <b>W2V2</b>		
	Delay 0.0 s	Delay 0.5 s	Delay 1.0 s	Delay 0.0 s	Delay 0.5 s	Delay 1.0 s
1.0	19.05	7.79	10.20	11.97	11.99	5.79
2.0	19.04	10.07	10.76	3.85	9.01	11.99
3.0	11.57	11.52	4.98	7.41	5.80	8.06
4.0	9.14	11.05	10.61	6.74	11.20	6.89

Table 16: Target-window WER (median, %) under cross-model transfer between W2V2 and HuBERT. Column groups follow the convention defined in Table 15: **W2V2** → **HuBERT** for W2V2-trained generator evaluated against HuBERT, and **HuBERT** → **W2V2** for the reverse direction. Window WER measures degradation localized to the 3-second perturbed segment.

Prefix (s)	<b>W2V2</b> → <b>HuBERT</b>			<b>HuBERT</b> → <b>W2V2</b>		
	Delay 0.0 s	Delay 0.5 s	Delay 1.0 s	Delay 0.0 s	Delay 0.5 s	Delay 1.0 s
1.0	55.6	20.0	33.3	40.0	54.6	12.5
2.0	53.9	33.3	30.0	11.1	44.4	50.0
3.0	30.0	30.0	12.5	33.3	25.0	28.6
4.0	14.3	33.3	50.0	33.3	54.6	33.3

The attack transfers effectively in both directions across the W2V2 and HuBERT pair in every configuration evaluated, with corpus-level attack WER between 3.85% and 19.05% against a clean baseline of ~2.0%—a 1.9–9.5× degradation on a model the generator never trained against. Across all 12 (prefix, delay) configurations, mean transfer attack WER is 11.3% from W2V2 to HuBERT (range 4.98–19.05%) and 8.4% from HuBERT to W2V2 (range 3.85–11.99%). This bidirectional transfer supports the architectural-family interpretation of CTC-based self-supervised models as a coherent target class: perturbations effective against one model exploit features that generalize to the other.

The strongest transfer occurs at short prefixes with zero delay. For **W2V2** → **HuBERT**, prefix = 1.0 s, delay = 0.0 s achieves 19.05% corpus WER and 55.6% median window WER, with 51.0% of utterances exhibiting  $\Delta\text{WER} \geq 0.10$ . This configuration also corresponds to one of the strongest in-domain configurations on W2V2 (Table 1), suggesting that the conditions which favor in-domain attack efficacy also favor transfer. The length-stratified breakdown reveals that medium-length utterances (6–15 words) are systematically more vulnerable to transferred attacks than long utterances (16+ words), with median  $\Delta\text{WER}$  on medium utterances reaching 30–47% at the strongest transfer configurations in either direction, mirroring the length-sensitivity pattern observed in the in-domain settings.

The transfer is asymmetric, with the W2V2 surrogate producing systematically stronger attacks on HuBERT than the reverse. Computing the transfer-retention ratio (transfer attack WER divided by in-domain attack WER) at delay = 0.0 s, both directions retain roughly comparable proportions of in-domain effectiveness at three of the four prefix lengths (44–58% retention), but diverge dramatically at prefix = 2.0 s: W2V2-trained perturbations retain 58% of their in-domain WER (32.72% to 19.04%), while HuBERT-trained perturbations retain only 15% (25.17% to 3.85%). Averaged across all 12 configurations, mean transfer attack WER is 11.4% from W2V2 to HuBERT versus 8.4% from HuBERT to W2V2—a 36% relative gap.

We hypothesize that the asymmetry arises from differences in the two surrogates’ pretraining objectives. W2V2 is trained via a contrastive objective on quantized speech representations, encouraging the encoder to learn linearly separable features at the frame level. HuBERT is trained to predict cluster assignments from offline-discovered acoustic units, which may produce more idiosyncratic decision boundaries that are harder for an external generator to find generalizable perturbations against. Adversarial perturbations crafted to exploit W2V2’s more linearly-structured representations may correspondingly transfer more readily to other CTC self-supervised models, while perturbations finding shortcuts in HuBERT’s specific cluster geometry are more model-bound. We do not have a definitive mechanistic test of this hypothesis, and we leave a more detailed analysis of surrogate transferability properties to future work.

A practical implication: practitioners deploying CTC-based ASR systems should expect W2V2-derived adversarial inputs to pose a broader threat than equivalent perturbations crafted against HuBERT, even when the deployed model is HuBERT itself.

#### H.4 Cross-Architecture Transfer to Whisper

Within the CTC self-supervised family, our attack achieves substantial transfer (Section H.3). To probe whether this transferability extends across architectural families, we evaluate against Whisper-small (17) – an encoder–decoder seq2seq model with a fundamentally different feature frontend and decoding pathway. We find a sharp architectural cliff: across four independently-designed black-box attack methods, all converge on attack WER within  $\sim 1\%$  of the clean baseline. We emphasize at the outset that this section’s purpose is to characterize the boundary at which CTC-trained attacks fail; the regime where our method’s advantage over baselines is established (substantial in-domain effectiveness on W2V2 and strong transfer to HuBERT, where our method outperforms a generic universal baseline by  $\sim 33\%$  relative on average) is reported in Sections H.3 and earlier.

To rule out alternative interpretations of the null transfer to Whisper – that it reflects a weakness specific to our generator-based attack, the LLM-forecasting step, or the W2V2 surrogate – we evaluate four black-box attack methods spanning two CTC surrogates and three target-knowledge regimes. Table 17 reports corpus-level attack WER for each method across the full prefix  $\times$  delay grid.

Across all 12 configurations and all four attack methods, attack corpus WER on Whisper falls within  $\sim 1.5$  percentage points of the clean baseline of approximately 4%, with mean  $\Delta$ WER ranging from 0.33% (SG with W2V2 surrogate) to 0.54% (Universal).<sup>2</sup> Window-level metrics are similarly unmoved: median target-window WER is 0% in all 48 (cell, method) combinations, and ASR@0.10 remains below 9% across the entire grid.

The convergent null result across four independently designed attack mechanisms isolates the architectural boundary as the dominant factor. Three orthogonal manipulations of the attack pipeline leave the null transfer intact: (i) substituting the LLM forecaster with oracle access to the target transcript (GT) does not improve transfer, ruling out the LLM-forecasting step as the bottleneck; (ii) substituting our generator-based attack with a generic input-agnostic universal perturbation does not improve transfer, ruling out a method-specific overfitting to W2V2; (iii) substituting the W2V2 surrogate with HuBERT does not improve transfer, ruling out a surrogate-specific shortcut. The CTC to seq2seq robustness gap thus reflects a genuine architectural-family boundary rather than a property of any particular attack design or surrogate choice.

Two architectural factors plausibly explain the absence of transfer to Whisper. First, Whisper is an encoder–decoder model with autoregressive token generation conditioned on a strong implicit language model, which can override locally corrupted acoustic evidence using surrounding context.

<sup>2</sup>Whisper’s clean WER on the LibriSpeech `test-clean` subset is higher than W2V2’s or HuBERT’s primarily because of occasional hallucinated tokens on short audio segments rather than systematic transcription errors.

Table 17: Cross-architecture transfer attack WER (%) on Whisper-small for four black-box attack methods. *SG (W2V2)* and *SG (HuBERT)*: our generator with LLM-forecasted target, trained against W2V2 and HuBERT surrogates respectively. *GT*: ground-truth oracle variant of our generator (LLM forecaster replaced with the actual target transcript). *Univ.*: input-agnostic universal adversarial perturbation. All methods at SNR=20 dB. Clean WER on Whisper is 3.91–4.17% across configurations.

Prefix (s)	Delay (s)	SG (W2V2)	SG (HuBERT)	GT (W2V2)	Univ. (W2V2)
1.0	0.0	4.90	4.76	5.31	4.87
	0.5	4.48	5.15	4.55	5.00
	1.0	4.40	4.21	4.56	4.52
2.0	0.0	4.50	4.27	4.57	4.78
	0.5	4.38	4.48	4.43	4.74
	1.0	4.43	4.36	4.52	4.48
3.0	0.0	4.31	4.48	4.24	4.55
	0.5	4.33	4.36	4.52	4.57
	1.0	4.16	4.18	4.26	4.42
4.0	0.0	4.10	4.35	4.31	4.32
	0.5	4.19	4.11	4.17	4.44
	1.0	4.23	4.37	4.21	4.30
<b>Mean</b>		<b>4.37</b>	<b>4.39</b>	<b>4.47</b>	<b>4.58</b>

Second, Whisper’s log-mel feature frontend and BPE tokenizer differ substantially from the raw-waveform CNN and character-level CTC heads of W2V2 and HuBERT, so perturbations crafted to manipulate frame-level CTC logits have no direct analogue in Whisper’s representational space.

This null result is consistent with the broader audio adversarial transfer literature, which has documented limited cross-architecture transfer between CTC and seq2seq ASR systems (1; 6; 35; 9). Combined with the strong bidirectional within-CTC transfer reported in Section H.3, the convergent results in Table 17 support an interpretation of attacks crafted against CTC self-supervised representations as exploiting acoustic features specific to that architectural family rather than generic distortions affecting any ASR system. We do not claim our attack is uniquely strong against seq2seq victims; the more substantive open question is whether *any* generator-based attack can bridge the CTC to seq2seq boundary, for instance via ensemble-surrogate training that incorporates a seq2seq model in the training loop. This and the related question of white-box attack ceilings against Whisper are natural extensions we leave to future work.

## H.5 Implications

The transferability profile suggests several conclusions for both attack design and threat-model analysis. First, an attacker need not have exact knowledge of the deployed CTC ASR model: a single CTC surrogate suffices to threaten an entire family of self-supervised CTC systems, with attack effectiveness reduced but not eliminated under transfer in either direction. Second, the choice of surrogate matters substantively even within the CTC family: W2V2 produces more transferable perturbations than HuBERT despite both belonging to the same architectural family. Third, defenders deploying seq2seq ASR systems such as Whisper appear to benefit from substantial robustness to perturbations crafted against CTC surrogates. Whether this advantage extends to perturbations crafted via *ensemble surrogate training*, in which the generator would be jointly optimized against W2V2, HuBERT, and Whisper losses, is a natural extension we leave to future work.